



JIMMA UNIVERSITY
JIMMA INSTITUTE OF TECHNOLOGY
FACULTY OF MECHANICAL ENGINEERING
MANUFACTURING SYSTEMS ENGINEERING

EXPERIMENTAL AND PARAMETRIC INVESTIGATION OF SUBMERGED FRICTION
STIR WELDING OF 6063 ALUMINIUM ALLOY

A Thesis Submitted to the post Graduate Studies, Jimma University, Jimma Institute of
Technology, faculty of Mechanical Engineering in Partial Fulfilment of the Requirements for the
degree of Masters of Science in Manufacturing Systems Engineering.

By:

Abenezer Abtaye

January 2023
Jimma, Oromia, Ethiopia

JIMMA UNIVERSITY
JIMMA INSTITUTE OF TECHNOLOGY
FACULTY OF MECHANICAL ENGINEERING
MANUFACTURING SYSTEMS ENGINEERING

EXPERIMENTAL AND PARAMETRIC INVESTIGATION OF SUBMERGED FRICTION
STIR WELDING OF 6063 ALUMINIUM ALLOY

A Thesis Submitted to the post Graduate Studies, Jimma University, Jimma Institute of
Technology, faculty of Mechanical Engineering in Partial Fulfilment of the Requirements for the
Degree of Masters of Science in Manufacturing Systems Engineering.

Main Advisor:

Dr.In. Mesay Alemu (Associate Professor)

Co-Advisor:

Mr. Lingerew Enbakom (M.Sc)

January 2023

Jimma, Oromia, Ethiopia

DECLARATION

This MSc thesis entitled as “Experimental and parametric Investigation of Submerged Friction Stir Welding of 6063 Aluminium Alloy” is the result of my own effort and has not been previously included in a thesis, exposition or report submitted to this university or to any other institution for degree, diploma or other requirement, excluding where due acknowledgement and reference is made. It is submitted to the Faculty of Mechanical Engineering, Jimma Institute of Technology, in partial fulfilment of the requirement for the award of masters of sciences in manufacturing system engineering.

By:

Abenezer Abtaye

Signature

Date

Main Advisor

Dr.In. Mesay Alemu (Associate Professor) _____

Signature

Date

Co- Advisor

Mr. Lingerew Enbakom (M.Sc)

Signature

Date

Internal Examiner

Name:

Signature

Date

External Examiner

Name:

Signature

Date

Chair person

Name:

Signature

Date

ABSTRACT

Several welding processes have been developed over time, however welding aluminium alloys has always been difficult using traditional welding techniques because of its low melting temperature. In addition to this some applications, such as underwater pipeline maintenance, automobile repair, and maritime engineering projects, demand underwater welding. Traditional welding methods, such as arc welding, could allow for this, but it is also a sophisticated and dangerous process because it allows the welder to work with electric equipment underwater. This study tried to overcome those problems by implementing the new SFSW process. SFSW is a relatively recent welding technology that is primarily used to join lightweight alloys such as aluminium alloys. The experiment was carried out on a 5 mm 6063 aluminium alloy sheet with a butt joint design. The investigation covers both experimental and numerical investigations. The influence of different welding parameters on thermal histories, tensile characteristics, and microstructural properties was investigated in the experiment. Finite element modelling was used in the numerical investigation to forecast changes in material properties and thermal profiles as the welding parameters vary. The following process parameters were used: (900, 1200, and 1400) RPM, (15, 30, and 45) mm/min tool speed, and straight cylindrical, taper cylindrical, and square tool profiles. According to the study's findings, the experimental and numerical tensile values of parent material were 163MPa and 171MPa, respectively. The maximum tensile strength of the experimental inquiry was achieved by combining 1400 RPM, 30 mm/min traverse speed, and straight cylindrical tool shape, yielding 151MPa. The most influential characteristics for successful SFSW operation and producing high mechanical attributes were discovered to be rotational speed. Under each parameter combination, the ABAQUS finite element model exactly predicted the temperature profile generated by SFSW.

Keywords: AA6063; *friction stir welding (FSW), submerged friction stir welding (SFSW/UFSW); orthogonal array; ANOVA; ABAQUS.*

ACKNOWLEDGEMENT

First and foremost, I want to express my gratitude to the Almighty God for providing me with the perseverance and patience necessary to overcome numerous challenges and complete my thesis.

Next, I want to express my gratitude to my adviser, Dr.In. Mesay Alemu(Associate Professor) for his help, patience, training chances, and vast knowledge. His guidance was helpful, and without it, I would not have been able to complete the task on time. Also, I'd like to express my gratitude to Mr. Lingerew Enbakom (M.Sc), my co-advisor, for his generosity and motivation. Finally I'd like to express my gratitude to Mr. Dk. Rao, Mr. Srinivasa R. K., and all of my classmates for their cooperation, assistance, and valuable input on my work.

ABBERRIVATION

FSW	Friction stir welding
SFSW	Submerged friction stir welding
UFSW	Underwater friction stirs welding
AAs	Aluminium alloys
HAZ	Heat affected zone
TMAZ	Thermo-mechanically affected zone
FS	Friction stir
AS	Advancing side
RS	Retreating side
ANOVA	Analysis of variance
EL	Eulerian Lagrangian
UTM	Universal testing machine

Table of Contents

DECLARATION	iii
ABSTRACT.....	iv
ACKNOWLEDGEMENT	v
ABBERIVATION.....	vi
LIST OF FIGURES	x
LIST OF TABLES	xii
CHAPTER ONE	1
INTRODUCTION	1
1.1 Background	1
1.1.1 Friction Stir Welding	1
1.1.2 Submerged Friction Stir Welding.....	2
1.2. Problem Statement	3
1.3. Objective of the study	4
1.3.1. General Objective	4
1.3.2. Specific Objective.....	4
1.4. Research Question.....	4
1.5. Significance of the study	4
CHAPTER TWO	5
LITERATURE REVIEW	5
2.1. Overview of FSW.....	5
2.2. Overview of SFSW	6
2.3. Advantages of SFSW over FSW	7
2.4. Process parameters of SFSW	8
2.5. Tool material and design	10
2.5.1. Tool shoulder diameter, D.....	11
2.5.2. Pin diameter, d.....	12
2.5.3. D/d ratio.....	13
2.5.4. Tool Pin length	13
2.6. Effect of parameters on the mechanical properties	13
2.7. Temperature distribution and measurement.....	14

2.7.1. Characteristic zones of FSW/UFSW	17
2.8. Residual stresses.....	18
2.9. Numerical Modelling FE Analysis.....	19
2.10. Welding Defects in SFSW	20
2.11. Summary of Literature Review and Research Gaps	22
CHAPTER THREE	23
MATERIALS AND METHODS.....	23
3.1. Materials.....	24
3.1.1. Tools and Equipment.....	24
3.1.2. Aluminium alloy -6063	26
3.1.3. Welding tool materials.....	27
3.2. Experimental Machine and setups.....	32
3.2.1. Welding Machine	33
3.2.2. Experimental Procedures	33
3.3. Inspection and testing.....	34
3.3.1. Tensile test.....	34
3.3.2. Liquid penetrant test	35
3.3.3. Microstructure	36
3.4. Determination of parameters with their levels	37
3.4.1. Determination of RPM levels	37
3.4.2. Determination of traverse speed levels.....	38
3.5. Optimization and Design of Experiments	39
3.5.1. Taguchi method	39
3.5.2. Selection of Orthogonal array.....	39
3.5.3. ANOVA Approach	40
3.6. Heat generation at tool-work Piece Interface.....	41
3.6.1. Contact shear stress	43
3.7. FE modelling	43
3.7.1 Material definition	46
3.7.2 Mesh description.....	47
CHAPTER FOUR.....	48

RESULTS AND DISCUSSION	48
4.1. Introduction	48
4.2. Experimental results	49
4.2.1. Tensile strength result	49
4.2.2. Liquid penetrant test result	51
4.2.3. Microstructure observation result	52
4.3. Effect of welding parameters on the temperature profiles	54
4.4. Effect of welding parameters on the joint quality	55
4.5. FE Result and Validation	58
4.5.1. Comparison of Experimental and Numerical result	60
4.6. Taguchi-based analysis	64
4.7. Analysis of S/N Ratios for UTS	64
4.8. ANOVA result	65
4.9. Verification/Confirmation Test	67
CHAPTER FIVE	67
CONCLUSION AND RECOMMENDATION	67
5.1. Conclusion	67
5.2. Recommendations and Future Work	69
REFERENCE	69
APPENDIX	76

LIST OF FIGURES

Figure 2. 1 Schematic view of FSW (Verma, Gupta, and Misra 2016).....	5
Figure 2. 2 Schematic view of SFSW (WAHID, KHAN, and SIDDIQUEE 2018).....	7
Figure 2. 3 FSW process parameters (Mohamadreza, Abbas S, and Spiro 2011).....	8
Figure 2. 4 Used pin diameter versus sample thickness (Venkateswarlu et al. 2013).....	12
Figure 2. 5 Peak temperature developed in AA 7055 during (a) FSW and (b) UFSW (Zhao, Wang, et al. 2014).....	15
Figure 2. 6 Different characteristic zones of FSW/UFSW (Threadgill 1997).....	17
Figure 2. 7 Temperature and stress field around a welding process (Williams and Steuwer 2010b).....	19
Figure 2. 8 welding defects in UFSW: (a) Furrow defect in AA 7055 (Wang, Zhao, Zhao, et al. 2015b); (b) Tunnel defects in AA 7055(Wang, Zhao, Zhao, et al. 2015b); (c) Groove defect in AA 2219 (H. J. Liu, Zhang, and Yu 2011); (d) Voids in AA 2219 (H. J. Zhang, Liu, and Yu 2011).....	21
Figure 3. 1 Study framework	23
Figure 3. 2 view of sample prior to welding and holding fixture	24
Figure 3. 3 Full setup used in the experimental work.....	25
Figure 3. 4 Dimension of aluminium used in the study	26
Figure 3. 5 H13 tool steel.....	28
Figure 3. 6 Design of the tools with their dimension in (mm).....	31
Figure 3. 7 Container and work piece holder/fixture	32
Figure 3. 8 Vertical Milling machine.....	33
Figure 3. 9 Size of the tensile specimen (ASTM E8-04).....	34
Figure 3. 10 AA6063 parent material and experimental test specimens	35
Figure 3. 11 Tensile test machine	35
Figure 3. 12 Steps in liquid penetrant testing	36
Figure 3. 13 Cleaner, Penetrant, and Developer	36
Figure 3. 14 Optical microscope.....	37
Figure 3. 15 Cause and effect diagram of parameters influencing SFSW joint strength.....	41
Figure 3. 16 Tool geometries: straight cylindrical, square and taper cylindrical tool	42
Figure 3. 17 3-D modelling of the Aluminium plate	46
Figure 3. 18 Eulerian- Lagragian assembly	46
Figure 3. 19 Assembly mesh model.....	48

Figure 4. 1 (a) before tensile test; (b) after tensile test	50
Figure 4. 2 Stress-elongation curve for 1200 RPM, 45mm/min Ts and straight cylindrical tool. 50	
Figure 4. 3 stress-elongation curve for 1400 RPM, 30mm/min Ts and straight cylindrical tool . 50	
Figure 4. 4 Stress-elongation curve for 900 RPM, 30mm/min Ts and taper cylindrical	51
Figure 4. 5 Liquid penetrant test results: (a) 900 RPM, 15mm/min, str. cyl; (b) 1200 RPM, 15mm/min, taper cyl; (c) 1400 RPM, 15mm/min, square tool and (d) after cleaning.....	51
Figure 4. 6 microstructure observation for: (a) 1200 RPM, 45mm/min, straight cylindrical pin; (b) 1400RPM, 30mm/min, straight cylindrical pin.....	52
Figure 4. 7 microstructure observation for: (a) 1200 RPM, 30mm/min, square pin; (b) 1400RPM, 15mm/min, square pin.	53
Figure 4. 8 microstructure observation for: (a) 1400 RPM, 45mm/min, taper cylindrical pin; (b) 1200RPM, 15mm/min, taper cylindrical pin.	53
Figure 4. 9 UTS vs RPM graph	57
Figure 4. 10 UTS vs Traverse Speed graph	57
Figure 4. 11 Geometry of the aluminium plate and tool.....	58
Figure 4. 12 Temperature contour at the beginning.....	59
Figure 4. 13 Temperature at various positions (ABAQUS)	59
Figure 4. 14 Temperature along the surface at rotational speed of 900 RPM	60
Figure 4. 15 Temperature along the surface at rotational speed of 1200 RPM	61
Figure 4. 16 Temperature along the surface at rotational speed of 1400 RPM	61
Figure 4. 17 FE test specimen after applying load.....	63
Figure 4. 18 FE test specimen at breaking stage.....	63
Figure 4. 19 stress-strain curve for experimental and numerical result for AA6063	63
Figure 4. 20 Main effects plot for S/N ratio.....	65
Figure 4. 21 prediction by Minitab	67

LIST OF TABLES

Table 2. 1 Types of FSW tools and materials joined (Chandrashekar, Kumar, and Reddappa n.d.; Joshi and Gandhi 2015).	11
Table 3. 1 Machines used in the study.....	25
Table 3. 2 Typical composition of Aluminium Al 6063 alloy (Davis 2001).....	26
Table 3. 3 Physical Property Aluminium Al 6063 alloy (Kaviyarasan et al. 2020)	27
Table 3. 4 Mechanical Property Aluminium Al 6063 alloy (Kaviyarasan et al. 2020)	27
Table 3. 5 Thermal Properties of Al 6063 alloy (Kaviyarasan et al. 2020).....	27
Table 3. 6 Chemical compositions of H13 tool steel (Said et al. 2015)	28
Table 3. 7 Mechanical properties of H13 tool steel (Said et al. 2015)	29
Table 3. 8 Characteristics and effects of different pin geometries on FSW process (Verma, Gupta, and Misra 2016).	30
Table 3. 9 RPM with UTS result	37
Table 3. 10 Traverse speed with UTS.....	38
Table 3. 11 Process parameters and their levels	40
Table 3. 12 Johnson-Cook parameters for plasticity of AA6063	47
Table 4. 1 Experimental result	49
Table 4. 2 Relation between parameters and temperature	54
Table 4. 3 Effect of weld joints.....	55
Table 4. 4 Experimental and simulated temperature comparison.....	62
Table 4. 5 Tensile result and S/N ratio	64
Table 4. 6 Response Table for Signal to Noise Ratios for Larger is better	65
Table 4. 7 ANOVA for Tensile Strength	66

CHAPTER ONE

INTRODUCTION

1.1 Background

1.1.1 Friction Stir Welding

Mechanical fastener-based joining was a crucial procedure for joining aluminium in the aerospace sector before friction stir welding was created. For example, the Eclipse Aviation industry used approximately 7,300 rivets per airframe to manufacture the Eclipse 500 business jets (Rajiv S Mishra and Sidhar 2016). The use of rivets also introduces unnecessary stress concentrators and may cause crevice corrosion and fretting corrosion. Therefore, it is not an economical way to use rivets as the connecting mechanism on the fuselage. After suffering such financial losses and physical harassment, Wayne Thomas of the Cambridge Welding Institute (TWI) in the United Kingdom invented the friction stir welding (FSW) in 1991 (Celik and Cakir 2016). Later, after the invention of this welding machine, the industry began to apply this method to make aluminium components such as deep-frozen hollow aluminium panels for ships, fuel tanks for spaceships, engine cradles for cars, etc., as well as in the space industry devices. It increases the strength of the body joint from 30% to 50%, the production time is reduced from 23 to 6 days, the energy consumption during the connection has dropped by about 50%, and the cost savings are up to 60% (Gibson et al. 2014; Verma, Gupta, and Misra 2016).

The base metal is softened during the friction stir welding (FSW) process, which uses friction heat to accomplish this. The term stir signifies the movement of the material in the form of plastic deformation. It is a welding process that utilizes the heat produced by the tool's friction with the BM and the plastic deformation of the BM caused by the stirring of the tool (Verma, Gupta, and Misra 2016).

When welding lightweight materials, a method of solid-state welding, known as friction stir welding, is gaining in importance. Both the heat produced by the friction between the work piece surface and the rotating tool and the heat generated by the plastic deformation of the material are sufficient to plasticize the work piece material to be joined and welded (Sun et al. 2017).

FSW is a welding technique that clamps two work parts together and welds them using a specially designed rotating tool. The force and heat generated by the friction of the work piece is applied by a rotary tool consisting of shoulders and pins. Friction raises the temperature of the work piece, softening the material but not melting it. The tool's rotation then stirs the material, allowing it to flow in plastic manner. This is called deformation at temperatures below the melting temperature of the material and causes various changes in its properties and microstructure.

The main advantage of FSW is its energy efficiency, environmental friendliness and versatility of "green" technology (Khan et al. 2015). Although the (FSW) process has many advantages, but this approach does not always produce defect-free joints. Defects such as wormholes, kiss bonds, route sticking, etc. Incomplete fusion wraps and flash formation can also occur (Singh, Singh, and Singh 2018).

1.1.2 Submerged Friction Stir Welding

One of the applications of FSW is that the ability of underwater welding is more feasible than underwater arc welding (Konkol and Mruzec 2007). The same tool and the same procedures used in air friction stir welding are used in SFSW. For the same material, different weld parameters; for instance, feed rate and rotational speeds, must be used to obtain the same quality as in air friction stir welding.

Since solid state welding occurs at a lower temperature than other traditional welding techniques, this newly developed welding technique can effectively weld aluminium alloys. FSW can be done using the same equipment that is used to weld samples in the open air and underwater. This gives friction stir welding an advantage over other welding methods, which can be difficult in the cases described previously. Plastic deformation causes many changes in the material's mechanical properties and microstructure during the process. The welding conditions, such as rotational speed, feed rate, and type of welding medium, influence these changes in properties (Eldin and Kishta 2014).

The underwater welding technology is critical for the construction of structures such as for underwater crude oil and natural gas extraction, as well as pipelines that carry gas or liquid under the sea. Furthermore, the erected structures could fail due to a variety of factors such as

corrosion, wear, and fatigue, among others. As well as for pipeline repair and operation, wet welding technology is applied in the process (Rogalski, Fydrych, and Łabanowski 2017).

1.2. Problem Statement

Over time, several welding procedures have been developed, but due to its high thermal conductivity and low melting temperature, welding aluminium and its alloys remains a challenge. In addition, some uses, such as repairing underwater pipelines, vehicles, and marine engineering ventures, necessitate underwater welding. This could be possible with traditional welding methods such as arc welding, but it is also a complex and hazardous technique since it allows the welder to work with electric equipment underwater. Underwater welding technology is of very much importance in the case of construction of structures like platforms for underwater mining of crude oil and natural gas as well as for erection of pipelines which transport gas or liquid under the water. Also, the erected structures may fail subjected to the various factors like wear, corrosion and fatigue, among others. Furthermore, maintenance and service of pipelines require a suitable wet welding technology. SFSW, a recently developed welding technique, can overcome both of these troublesome welding situations.

1.3. Objective of the study

1.3.1. General Objective

The major goal of this study is to investigate the effects of weld parameters on submerged FSW and their effects on the mechanical properties and microstructure of the material.

1.3.2. Specific Objective

To attain the general objective, the following specific goals were identified.

- ✓ Determine the mechanical properties of the weld, conduct tensile tests on the welded samples and constructing the stress strain(S-S) curve.
- ✓ Conduct microscopic photographs to investigate the effect of factors on the material's microstructure.
- ✓ Conduct (non-destructive test) liquid penetrant test.
- ✓ Examine the impact of process parameters on the outcomes and finding the most influential combination of parameters Using ANOVA.

1.4. Research Question

The study was to answer the following research questions:

- ✓ What are the most important study procedure parameters that give 6063 AA material its maximum tensile strength?
- ✓ Which combination of weld parameters produces the best weld surface?
- ✓ Which optimization strategies are appropriate for a multi-response experiment?
- ✓ Which weld parameters have the greatest impact on weld quality?
- ✓ What is the effect of SFSW on mechanical property and microstructure of the weld?

1.5. Significance of the study

The importance of this study can be described in terms of its use in providing information to industry sectors and researchers. The study is useful in both theoretical and practical terms, and it can fill a void in the literature. It comprised welding instructions, as well as experimental setup and results in relation to welding process parameters.

CHAPTER TWO

LITERATURE REVIEW

This chapter provided basic knowledge from literatures related to the process parameters of both frictions stir welding and UFSW.

2.1. Overview of FSW

Friction fusion welding is a solid state welding process that can efficiently overcome the weaknesses of traditional fusion welding technology (H. Zhang and Liu 2013).

The basic principle of using a FSW is using a rotating tool, made of materials stronger than the work piece and a specially designed tool shoulder and pin profile. The tool pin is plunged into the work piece at a pre-programmed depth and the shoulder surface contacts with the work piece. The work pieces heated below the melting point and the softened materials moved from the front to the backside, as well as from top to bottom. It also provides agitation in the nugget zone during the process. The tool rotates clockwise and moves from the front of your foot to the back. The left side, where the rotational direction of the tool coincides with the direction of movement of the tool, is called the advance side. The side opposite to the moving side, where the rotation of the tool is opposite to the direction of movement of the tool, is called the backing side (Rajiv Sharan Mishra, De, and Kumar 2014). Below figure is schematic view of friction stir welding.

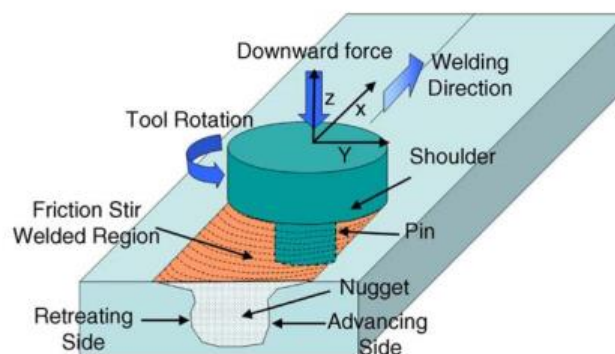


Figure 2. 1 Schematic view of FSW (Verma, Gupta, and Misra 2016)

2.2. Overview of SFSW

(Upadhyay and Reynolds 2010) examined the influence of thermal boundaries on FSW and SFSW. Friction stir welding was performed on samples in air and samples immersed in water to determine the effect of quenching rate on joint performance and some welding response parameters. It was found that the maximum temperature of the sample welded in air and the sample immersed in water during the welding process was almost the same; however, the cooling rate of the immersed sample was higher than that of the sample welded in the air. In addition, the submerged arc friction stir welding samples had a smaller grain size than the samples obtained by air welding. It also demonstrates that underwater welded specimens have a higher tensile strength than air welded specimens, and this has been proven experimentally. Despite lowering the welding temperature by submerging the sample, it was observed that the sample required more torque to stir the material; this required more rotations and thus required more power consumption.

(H. J. Zhang, Liu, and Yu 2011) studied the effects of rotational speed on welding by incorporating submerged friction of aluminium alloys. The material used in the study is the aluminium alloy 2219-T6. The shoulder diameter of the welding tool used was 22.5 mm, and the pin diameter and length were 7.4 mm. It shows that the tensile strength of the weld increases as the speed increases from 600 rpm to 800 rpm; then, as the speed increases from 800 rpm to 1200 rpm, it remains unchanged, and finally, as the speed reaches 1400 rpm, it drops sharply; there is a void defect on the weld. The increased rotation speed softens the material and provides better agitation.

Other researchers studied the effect of water temperature on the quality and properties of the weld (Rui-dong et al. 2011). A sample of 7050 aluminium alloy was friction stir welded in air, and then submerged in cold and hot water. The results show that hot water is the best welding environment, where the tensile strength of the weld was 92% of the tensile strength of the untreated material, and the ductility increased to 150% compared to the untreated sample. The tensile strength of the cold water and air welded samples fell to approximately 85% and 75%, respectively, of the raw sample; whereas ductility in air has increased by 30% and in cold water by 25% compared to the raw sample. These outcomes are consistent with the results of another study conducted by (H.-J. Liu et al. 2010). This also confirms that, compared with traditional

friction stir welding, immersion friction stir welding has a positive effect on the tensile strength of the material.

Submerged friction stir welding has greater weld force than FSW. This is due to the fact that the amount of weld power utilized is related to the torque magnitude. To deal with the water head, the torque value is larger in the submerged friction stir welding process. The higher torque extracted by the tool necessitates greater motor power. As a result, weld power consumption in the SFSW technique increases.

(Hofmann and Vecchio 2005) Used submersion as a way to increase the rate of cooling of the sample and reduce its exposure to high temperatures. It has been shown that the process radically reduces the proportion of conductive heat flow in the process. Due to this reduction in conduction heat, the average particle size became smaller, and we were able to achieve a particle size of 200 nm or less. Below is Schematic view of SFSW.

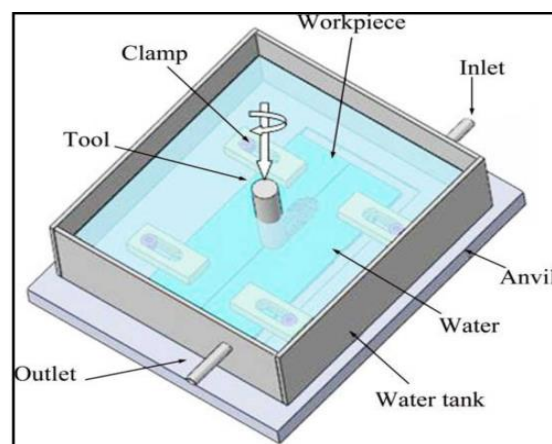


Figure 2. 2 Schematic view of SFSW (WAHID, KHAN, and SIDDIQUEE 2018)

2.3. Advantages of SFSW over FSW

Due to its capacity to give higher mechanical qualities over FSW, UFSW is becoming a very important welding method (Mofid et al. 2012). (WAHID, KHAN, and SIDDIQUEE 2018) compared UFSW to FSW and FW in terms of numerous elements in order to show the advantages and benefits of UFSW over SFSW. Then they have concluded on below points:-

- ✓ SFSW prevents oxidation and provides a better surface finish than FSW.
- ✓ UFSW is appropriate for overheating-sensitive materials and alloys..

- ✓ SFSW presents a refined grain structure compared to FSW.
- ✓ The maximum (peak) temperature of SFSW is lower than that of FSW, which limits coarsening and precipitate dissolving.
- ✓ Compared to FSW, SFSW offers greater mechanical qualities for the weld plate.
- ✓ Because it reduces softening, UFSW is better suited to heat-treatable aluminum alloys.
- ✓ Welding defects are less common in UFSW than in FSW.
- ✓ Compared to FSW, UFSW decreases residual loads and produces less distortion.

2.4. Process parameters of SFSW

Taguchi divides factors/parameters into fixed factors and controllable factors. Fixed factors are factors that affect the outcome of a product or process, but are usually not maintained at a particular level during the manufacturing process or application period. Controllable elements, on the other hand, are elements that can be levelled and controlled during the experiment and in the final design of the product or process (Roy 2010). Both in FSW and SFSW, the joint configuration is dominated by the effect of material flow and high mechanical deformation. Several parameters were taken into account in SFSW for high weld quality. In this study, the parameters are categorized into controllable and fixed parameters based on the availability of materials and tools.

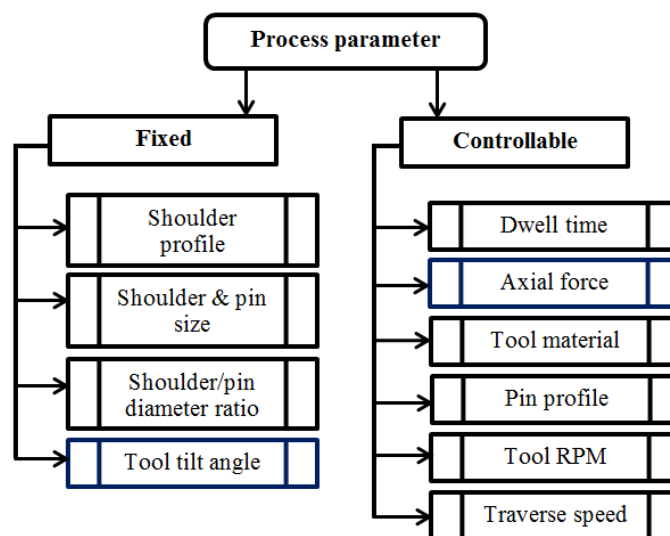


Figure 2. 3 FSW process parameters (Mohamadreza, Abbas S, and Spiro 2011)

(Verduzco Juárez et al. 2016) investigated how process variables affected friction stir welding of 6061-T6 aluminium alloy with a butt weld configuration. The process was performed at a rotation speed of 800, 1000, 1200 rpm, a traverse speed of 40, 90 mm/min, a penetration speed of 3,9 mm / min, and an axial force of 8 KN. They used H13 tool material to obtain a maximum tensile strength of 177 MPa at a tool speed of 1200 rpm, and observed a minimum tensile strength of 108 MPa when using 9840 tool steel at 1,200 rpm.

Process parameters for FSW improvement on 6061-T6 aluminium alloy material with butt joint configuration were investigated by (Gomathisankar, Gangatharan, and Pitchipoo 2018). The maximum tensile and hardness strength with a defect-free joint were obtained at 560 and 710 rpm with a value of 230 MPa and 55.33 HV respectively.

(Shinde and Rathi 2016) were trying to increase the joint strength of FSW by optimizing the process parameters of FSW in a 6 mm 6061 aluminium alloy with a butt joint configuration. Three different speeds of 1000, 1500 and 2000 rpm with a travel speed of 30, 35 and 40 mm/min and tool inclination angles of 0, 1 and 2 degrees are recorded. And maximum tensile strength of 132 N/mm² at a travel speed of 30 mm/min at a speed of 2000 rpm is achieved.

The effect of different tool pin clips on the 4.75 mm thickness of 6063-T6 AA material with butt joint formations was investigated by (Hussain et al. 2018). The experiment was carried out with a high performance vertical milling machine and five different pin profile tools were used, namely conical cylindrical, straight cylindrical, straight square, hexagonal and triangular tools. The parameters of the process are that the tool rotates at 900 rpm, the tool moves at 50 mm/min, and the tool tilts at an angle of 1.5°. The welds on these joints were fabricated with a tapered cylindrical tool, which yielded an increase in tensile strength and impact energy by 162 MPa and 26 joules, respectively. The lowest tensile strength observed on the triangular tool was 115.6 MPa, and due to improper material flow and ineffective consolidation, tunnel defects were found on the forward side of the joint made with this pin profile.

The effect of dwell time on the evolution of the microstructure and mechanical properties of stirred friction contrast spot welding with dwell time of 1, 5 and 9 s was studied by (Li et al. 2019). It is found that longer dwell time leads to a higher temperature peak and vice versa. The effects of process parameters on friction stir spot welding of aluminium alloy materials with

dwel times of 1, 5 and 10 seconds at immersion speeds of 5, 10 and 15 mm/min was examined by (Chen, Liu, and Ni 2017). It is concluded that the amount of time a joint is in contact with a surface is more influential factor in determining joint strength than the speed at which a joint penetrates a surface.

The effects of axial force on the mechanical properties of AZ80A Mg materials were examined with three distinct axial force values of 1, 2, and 3 KN by (Sevvel and Jaiganesh 2017). By using the specifications of a 3 KN axial force, 750 rpm tool rotating speed, and 75 mm/min feed rate, they were able to achieve a greater tensile strength of 234 MPa.

2.5. Tool material and design

Tool wear and weld quality are two key factors to consider when choosing a tool material, since their qualities can influence weld quality by influencing heat generation and dissipation. Interaction with degraded tool material may potentially impact the weld's microstructure.

Aside from the potential for negative impacts on the weld microstructure, substantial tool wear raises the cost of processing FSW. Temperatures in the work piece are influenced by material qualities of the tool, such as thermal conductivity, and processing parameters for a certain work piece (Besharati-Givi and Asadi 2014).

The material a tool's made from is important to determine whether or not the tool will be suitable for welding a particular material.

- ✓ Excellent strength and wear resistance at high temperatures to withstand high plunge forces,
- ✓ good coefficient of friction to the work piece for sufficient frictional heat generation,
- ✓ Good dimensional stability, reusable.
- ✓ The machinability for making complex geometry is good.
- ✓ Should not react with oxygen and work piece material,
- ✓ Hot hardness must be high to complete the long and cost-effective welding (Joshi and Gandhi 2015; Meilinger and Török 2013).

A variety of materials are available for a variety of materials and applications.

Table 2. 1 Types of FSW tools and materials joined (Chandrashekar, Kumar, and Reddappa n.d.; Joshi and Gandhi 2015).

No	Tool materials	Materials welded	Characteristics
1.	HCHCr	AA5083-H111 Al alloy and Magnesium alloy	High wear resistance.
2.	SS310	Commercial grade Al-alloy 6 mm thick and Magnesium alloy	Very high corrosion resistance.
3.	H13	C11000 and AA5754 copper with thickness of 3.175 mm	-
4.	HSS	AA2011, AA6063 alloys 10 mm thick and Magnesium alloy	High wear-resistant.
5.	C40	AA6082 and AA2024 4 mm thick	-
6.	H13	6061-T6 Al and AISI 1018 mild steel 6 mm thickness and Magnesium alloy	Shock and abrasion resistance combined with red hardness.
7.	SKD61 tool steel	For dissimilar materials	Good thermal fatigue resistance
8.	Armour steel	For Magnesium alloy	-
9.	Mild Steel	For Magnesium alloy	-
10.	AISI oil hardened tool steel	For aluminum matrix composite materials	-
11.	AISI 4341	Widely used for Al, Mg, Cu, Al/Mg-MMC	Good elevated temperature strength.
12.	High Carbon Steel	For Magnesium alloy	-
13.	PCBN	Cu, Ti, Ni alloys, steel, and AlMMC	Chemical stability, excellent wear resistance at elevated temperature.

Tool design is a critical factor during FSW and plays a vital role in the process and in the mechanical properties of the plasticized material. FSW tools are designed to heat plastic and metal by rubbing between the tool and the material. The tool consists of two main parts: the tool shoulder and the tool pin (Khan, Siddiquee, and Khan 2017).

2.5.1. Tool shoulder diameter, D

Tool shoulders are designed to induce frictional heating of the work piece's surface and subsurface regions. In the welding of thin metal sheets, the tool shoulder is responsible for the majority of the deformational and frictional heating (Shercliff et al. 2007).

(Elangovan and Balasubramanian 2008) Attempted to understand the effect of tool pin profile and tool shoulder diameter on friction stir process zone formation on (300*150*6 mm, L*W*T) of 6061 AA materials with butt joint configurations. They used variables that were both controlled and fixed. Tool rotating speed of 1200 rpm, traverse speed of 75 mm/min, and axial force of 7 KN are all adjustable parameters. The joints were made using fixed parameters such as tool D/d ratios of 2.5, 3.0, and 3.5 with a pin length of 5.5 mm, tool shoulder diameters of 15, 18, and 21 mm, pin diameter of 6 mm, and five different tool pin profiles: straight cylindrical, tapered cylindrical, cylindrical threaded, triangular, and square. The paper's findings revealed that employing a square pin shaped tool with an 18 mm shoulder diameter imparted maximum tensile strength and defect-free welds when compared to other methods.

2.5.2. Pin diameter, d

One of the most important parameters influencing the tensile strength of the joint metal and the cross-sectional area of the weld is pin diameter. This is due to the fact that the solder fluctuation is primarily produced by the activity of the pin (Venkateswarlu et al. 2013).

The influence of the FSW tool design on the mechanical characteristics of AA2198-T3 and AA2024-T3 welded joints is presented by (Khalilabad et al. 2016). They stated that the maximum pin outer diameter is determined from $0.8 * \text{plate thickness (mm)} + 2.2$ and the minimum pin diameter is also calculated from $0.5 * \text{plate thickness}$.

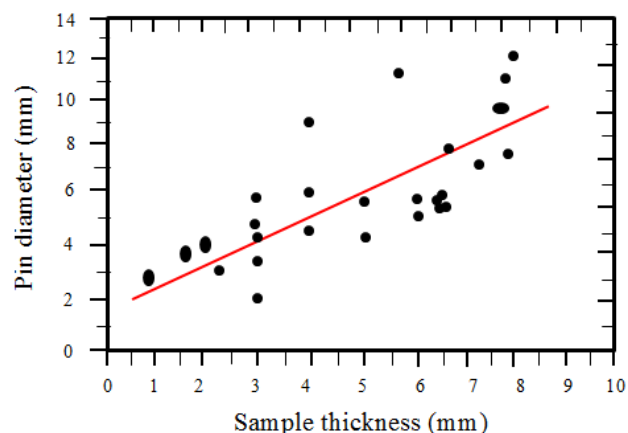


Figure 2. 4 Used pin diameter versus sample thickness (Venkateswarlu et al. 2013)

(Dubourg and Dacheux 2006) reviewed the design and characteristics of FSW tools. They pointed out that for sheet thicknesses of 1 to 8.3 mm; the pin diameter is the closest or equal to the work piece thickness. Unless the agitation process is ineffective, it is about 3mm in addition to the minimum pin diameter. For example, for a plate weld with a thickness of 8 mm, the pin diameters range from 8 to 13 mm, resulting in a defect-free weld.

2.5.3. D/d ratio

It is the ratio of the diameter of the shoulder divided by the diameter of the tool pin. It plays an important role during plastic deformation during agitation, and as a result, its value is carefully selected to obtain the desired result.

(Khan, Khan, and Siddiquee 2015) used four different D/d ratios such as 3.2, 3, 2.8, and 2.6 for the effect of the ratio of shoulder diameter to pin diameter to 6063 aluminium alloy material and joints. The results showed that a D/d ratio of 2.6 gave the highest tensile strength of 145.34 MPa and a lower D/d ratio of 2.8 described a lower tensile strength of 135.4 MPa. The effect of the ratio of shoulder diameter to pin diameter to different aluminium materials in AA2024-T6 and AA7075-T6 is studied by (Saravanan et al. 2016). The results show that, compared with other joints, the joints made with a D/d ratio of 3 exhibit better mechanical properties.

2.5.4. Tool Pin length

A major factor in designing an FSW tool is the pin or screw length. If the lead length is equal to the thickness of the base material, welding will be invalid. There are two ways that the pin can touch the support plate: it can both touch the support plate and cause material congestion so the shoulder doesn't touch the surface, or it can make contact without causing any material congestion. According to the study of (Meilinger and Török 2013), the lead length must be 0.3 mm smaller than the thickness of the base material. At this length the shoulder touched the surface and the root was good.

2.6. Effect of parameters on the mechanical properties

According to the reviewed literature (in water and other liquid medium), most researchers compared the mechanical qualities of welded joints created by conventional FSW (in air) with submerged FSW.

In both FSW and SFSW, the key process parameters under investigation are tool rotational and tool traversal speeds. The experiments revealed that the welding traversing speed plays a significant effect in improving the mechanical properties of UFSW joints (N D Ghetiya and Patel 2015). When the tool rotating speed was increased and the tool traversal speed was decreased, the TS increased (Wang, Zhao, Zhao, et al. 2015a). Lower rotating speeds and greater traversal speeds produce finer grains in the welded zone, increasing toughness (Bijanrostami and Vatankhah Barenji 2019). In FSW in the air, a faster tool travel speed lowers the heat input, which lowers the dissolution, which strengthens precipitate formation and so increases the TS. Due to the creation of voids, both lower and higher tool travel speeds decrease TS in the case of UFSW (Nilesh D Ghetiya and Patel 2017). In addition, raising the traversing speed increases the welded joint's efficiency by 20-25 percent in UFSW (Sabari, Malarvizhi, and Balasubramanian 2016a).

(Rui-dong et al. 2011) tested FSW in three different environments: air, cold water, and hot water. They came to the conclusion that, regardless of the weld parameters utilized, the FSW performed under hot water conditions was the most effective in enhancing the welded joint of the three. According to (Sabari, Malarvizhi, and Balasubramanian 2016b) the tensile strength (TS) of a joint manufactured in UFSW is stronger, and the joint efficiency is around 60% higher than that of a joint made in FSW. The higher tensile strength is due to the sequence of precipitation formation and heat accessible in the thermo-mechanical affected zone (TMAZ). As a result of the greater cooling rate in UFSW than in traditional FSW, the weld became brittle and tensile strength increased, as found by (Papahn et al. 2015). A tensile strength of 152.3 MPa in FSW of dissimilar materials, i.e., Al and Mg alloys, which is 63.3 percent of Mg alloy sheet strength was reported.

2.7. Temperature distribution and measurement

The temperature in the weld zone has a direct relationship with the microstructure (grain size, coarsening of the precipitates) and mechanical qualities of friction stir (FS) welds. Weld temperature measurements are problematic in FSW because the weld zone generates a lot of heat due to the strong plastic deformation at the work piece-tool contact, which is the hottest area of the weld. It's also difficult to establish the SZ temperature because of the tool probe's spin. Implanted temperature devices (thermocouples) in the work piece are the most commonly

utilized temperature measuring techniques during FSW (H. J. Zhang, Liu, and Yu 2012). In FSW, cooling medium has a significant impact on the temperature profile; as well as in the ensuing microstructure and strength. As a result, understanding the temperature distribution throughout the cooled joints is critical to understanding the importance of UFSW.

Due to the great heat absorbing capacity of water, the UFSW sample has a lower peak temperature than the FSW sample, resulting in improved UFSW joint characteristics (Kishta and Darras 2016; H. J. Zhang, Liu, and Yu 2012). UFSW also results in higher heating and cooling rates, which leads to a shorter dwell time above a given temperature and a lower peak temperature (H. J. Zhang, Liu, and Yu 2012).

(Zhao, Wang, et al. 2014) Used UFSW to improve the joint performance of spray formed Al 7055 alloy by altering the temperature history. The temperature was measured using eight thermocouples, four on the advancing side (A1-A4) and four on the retreating side (R1-R4). Due to the extra heat taken away by the water, the maximum temperature measured in water was 68.5 °C, which was 118 °C lower than in air. Figure 2.5 depicts AA 7055's peak temperature patterns in FSW and UFSW. Moreover, the temperature range measured during FSW on AS and RS showed a huge decline and large thermal gradient, in contrast to UFSW, which showed a much smaller reduction in temperature. Because of the lower temperature and lower thermal gradient caused by water cooling, the coarsening of strengthening precipitates was minimized, resulting in better joint characteristics. Figure 8 depicts the thermal gradient profile in FSW and UFSW.

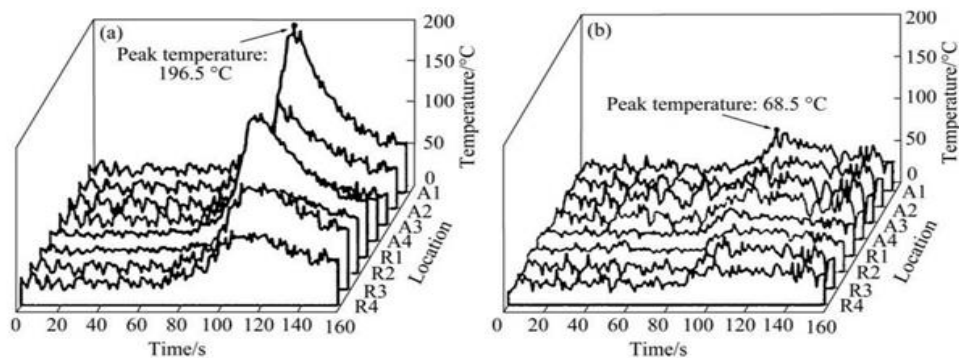


Figure 2. 5 Peak temperature developed in AA 7055 during (a) FSW and (b) UFSW (Zhao, Wang, et al. 2014)

(Rui-dong et al. 2011) investigated the temperature, strength, and elongation behaviour of AA7050 using three distinct fluids (air, warm, and cold water). The temperature of the weld was measured using eight channel thermo detectors. The following tests were discovered:

- ❖ The sample welded in air reached the maximum peak temperature of 380 °C. In cold and hot water, the welded samples reached peak temperatures of around 220 and 300 °C, respectively;
- ❖ Due to the constraint, it imposes on coarsening of second phase strengthening particles in heat affected zone. The use of warm water resulted in the greatest mechanical strength and elongation.
- ❖ When compared to air, cold water increased tensile strength and decreased elongation. The hardening of the weld joint resulted in decreased elongation due to the low temperature achieved in cold water.

By managing the temperature, water cooling improves the mechanical qualities of the HAZ (Mofid et al. 2012). The coarsening and dissolving of the precipitate is hampered, and the breadth of the precipitate free zone (PFZ) is also regulated in UFSW of AA 2219, resulting in a hardening improvement in the HAZ. Several more studies have confirmed the beneficial effect of liquid cooling on the improvement of strength in FSW joints (Mofid et al. 2012; Wang, Zhao, Zhao, et al. 2015a; H. J. Zhang, Liu, and Yu 2012). The controlled temperature distribution and thermal profiles result in cooling action (water), which improves strength. Furthermore, due to water cooling, the low peak temperature created during UFSW can minimize the development of intermetallic compounds (IMCs) in Al-Mg (Zhao et al. 2015, 2016). In UFSW, the maximum peak temperature is in RS, but in FSW, the maximum peak temperature is in AS, as seen in some 7xxx alloys (Rui-dong et al. 2011; Wang et al. 2016). In FSW, the AS is deformed more than the RS, resulting in a higher temperature on the AS. In UFSW, the heated water near the weld is propelled to travel forward on AS, confronting the cold water close to the weld, and chills down instantly and mandatorily, while RS receives the heated water from AS, resulting in a high temperature on RS. Welding settings have an impact on temperature profiles as well.

Changes in welding speed have a greater impact on thermal cycles of joints in water than changes in rotation speed, yet rotation speed can afford a wider adjustment range than welding speed for the UFSW process (Wang, Zhao, Zhao, et al. 2015a). Increased rotational speed

allows for rapid cooling and a high peak temperature. In comparison to FSW, UFSW requires a higher welding and rotational speed. Heat generation affects the forces that occur on the tool, as well as the temperature distribution in UFSW/FSW (Papahn et al. 2015). Because of the lower peak temperature, the axial and translational forces in UFSW of AA 7075-T6 are greatly improved.

2.7.1. Characteristic zones of FSW/UFSW

The first to characterize the microstructure of friction stir welding was (Threadgill 1997). Its research was limited to AAs, and because their behaviour differs from that of other materials and alloys, this characterisation was deemed insufficient. As a result, new words were developed, which were later amended and incorporated into American Welding Society Standard D17.3M (American Welding Society 2006). The proposed concepts are depicted in figure 2.6 and are discussed in the following manner.



Figure 2. 6 Different characteristic zones of FSW/UFSW (Threadgill 1997)

- 1) Unaffected material or parent metal: no plastic deformation occurs, but the material may or may not have been affected by the welding heat. There is no discernible change in characteristics or microstructure.
- 2) Heat-affected zone (HAZ): This zone is impacted by welding heat, although there is no visible plastic deformation in this zone.
- 3) Thermo mechanically impacted zone (TMAZ): The material is affected by both plastic deformation and thermal cycles in this zone. In AAs, a sharp and unambiguous boundary separates the deformed and recrystallized regions of TMAZ (this region is commonly referred to as 'nugget'). Other names for this region include SZ and 'dynamically recrystallized region' (American Welding Society 2006).

The mechanical properties of the welds generated are directly affected by changes in microstructure of different zones. The development of distinct textures (XU WF et al. 2012) and precipitate dissolution and coarsening in separate zones occur as a result of the high heat and strong deformation experienced during FSW/UFSW (H. J. Liu, Zhang, and Yu 2011; Sabari, Malarvizhi, and Balasubramanian 2016b; H. J. Zhang, Liu, and Yu 2012). Many scholars have looked into different microstructural changes in FSW/UFSW. Various studies have examined the effect of coolant (water and air) on grain boundary phases, grain size, defects, and development of intermetallic compounds (IMCs) (XU WF et al. 2012; Zhao, Zhou, et al. 2014).

2.8. Residual stresses

Remaining forces in a material after all external forces have been eliminated are known as residual stresses (RS). They develop as a result of inhomogeneous deformation that has mechanical, thermal, or micromechanical roots.

Due of the enormous impact residual stresses from welding have on component life and distortion, they have been the focus of in-depth study and published literature. On FSW 2024Al-T3 and 6013Al-T6 joints, (Dalle Donne et al. 2001) assessed the residual stress distribution using several approaches. They discovered that longitudinal and transverse residual stresses are distributed in "M" pattern across the weld. Furthermore, regardless of traverse speed, tool rotation speed, or pin diameter, longitudinal residual stresses are greater than transverse residual stresses. (Peel et al. 2003) measured the residual stress in FSW AA5083 welded joints using the synchrotron X-ray method. The findings demonstrate that the weld bead is under tension in both the longitudinal and transverse residual stress directions. They have also demonstrated that as traverse speed increases, longitudinal tensions increase as well.

An uncoupled thermo-mechanical model for various aluminium alloys and 304 L stainless steel has been created by (Khandkar et al. 2006) based on torque input for estimating temperature and then residual stress.

Figure 2.7 depicts the heat and stress fields near the weld zone. Due to the thermal expansion of the warming (and consequently expanding) material that is being restrained by the surrounding cold material, there is a significant area of compressive stress in front of the weld zone. Plastic

flow happens when the tension is greater than the compressive yield stress (Williams and Steuwer 2010a).

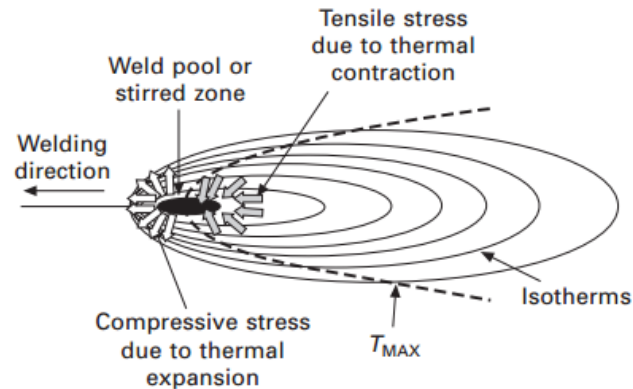


Figure 2. 7 Temperature and stress field around a welding process (Williams and Steuwer 2010b)

2.9. Numerical Modelling FE Analysis

(Hattel Schmidt and Hattel 2004) Developed a thermo-mechanical model to study the parameters under which FSW can create a flawless weld with no void. To avoid significant mesh distortion owing to high plastic deformation, the model was created using the commercial software ABAQUS/Explicit with ALE formulation and re-meshing option. According to the sticking and sliding circumstances at the time, heat created in the process is due to plastic dissipation and frictional dissipation. The mesh quality was lowered in this work to reduce the simulation time, which was reported to be 14 days for a 10 second simulation on a high-speed computer.

(Tolcha and Melaku 2020) developed a thermal model for friction stir welding of AA 6061. Using 3mm thick aluminum sheet as the lagrangian (work piece) and various welding techniques, a coupled Eulerian-Lagrangian (CEL) formulation was created. FEM simulation was successfully completed using ABAQUS 6.14/explicit software, yielding a maximum temperature of 546⁰C. When the cooling rate was slow, it was discovered that joint defects such as tearing, hot cracking, and residual thermal stress were reduced.

(Z. Zhang and Zhang 2009) created another thermo-mechanical model to anticipate differences in thermal history and material due by various welding parameters in friction stir welding. The model was created using ABAQUS/Explicit commercial finite element analysis software. To

avoid excessive element distortion in the mesh due to high plastic deformation, an arbitrary Lagrangian-Eulerian (ALE) formulation was utilized. Furthermore, mass scaling was found by comparing internal and kinetic energy to avoid element distortion. The model correctly predicted findings that were equal to the experimental results; it was stated that as the rotating speed increased, so did the welding temperature. Increasing the rotational speed raises the power consumption and residual strains on the sample.

Despite the fact that various studies have been undertaken on the subject, only a few of them have focused on submerged FSW. The current study aims to better understand the effect of submerging on FSW, as well as the effect of welding parameters such as rotational speed and feed rate on submerged FSW.

2.10. Welding Defects in SFSW

In FSW/UFSW, many defects like (voids, grooves, tunnels, kissing bond, etc...) have been discovered by the following studies (Khan et al. 2015; H. J. Zhang, Liu, and Yu 2011; H. Zhang and Liu 2012). The material flow in FSW/UFSW is governed by welding settings as well as the cooling medium. If the plasticized material is allowed to cool before filling the joint behind the tool, defects can emerge. If the welding settings are not chosen properly, defects usually emerge as a result of an incorrect rate of heating. Furrow flaws and voids are common in UFSW when the rotational speed is too low or too high, respectively. Insufficient material flow causes these flaws, which can be seen on the weld's surface or beneath it. During UFSW, a furrow defect is detected in AA 7055 in SZ at low rotation speed (Wang, Zhao, Zhao, et al. 2015a), while voids are observed in the SZ at too high rotation speed in AA 2219 (H. J. Zhang, Liu, and Yu 2011; H. Zhang and Liu 2012). Increasing the rotational speed from a lower to a higher value reduces or removes these faults, whereas increasing the rotational speed from a higher to a higher level increases the size of the voids (H. Zhang and Liu 2012).

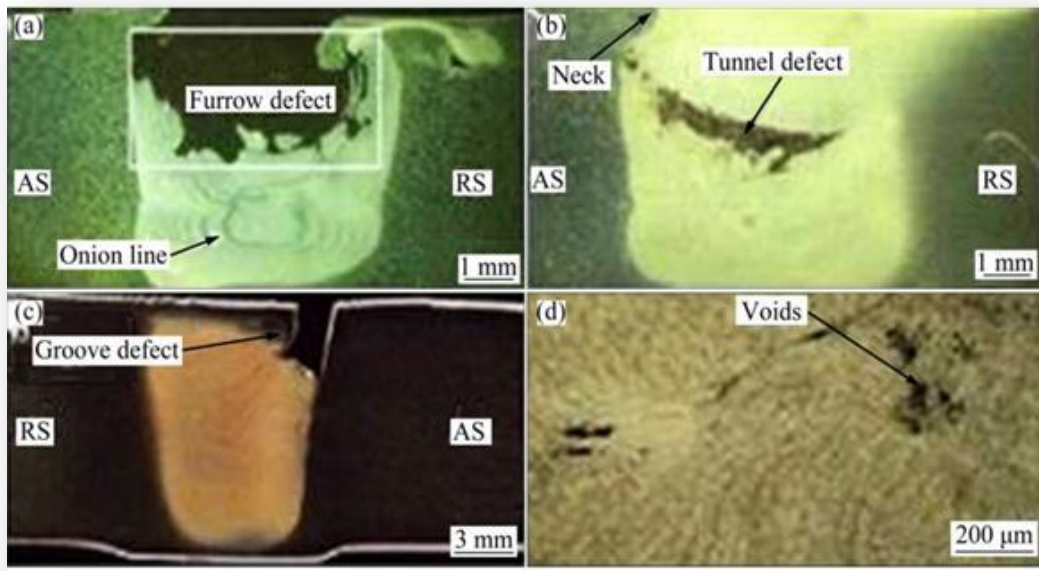


Figure 2. 8 welding defects in UFSW: (a) Furrow defect in AA 7055 (Wang, Zhao, Zhao, et al. 2015b); (b) Tunnel defects in AA 7055(Wang, Zhao, Zhao, et al. 2015b); (c) Groove defect in AA 2219 (H. J. Liu, Zhang, and Yu 2011); (d) Voids in AA 2219 (H. J. Zhang, Liu, and Yu 2011)

In the SZ, problems have also been discovered due to excessive welding speed (H. J. Liu, Zhang, and Yu 2011; Wang, Zhao, Zhao, et al. 2015a). Tunnel defect and grove defect are detected in AA 7055 (Shinde and Rathi 2016) and AA 2219 in UFSW at high welding speeds (H. J. Liu, Zhang, and Yu 2011). Plasticized material cools quickly in water at high welding speeds before entirely filling the weld, resulting in a tunnel defect. Due to insufficient frictional heat, tunnel flaws are also detected in the SZ of the joints at the AS created using straight and taper cylindrical tools in AA 2519 T-87 (Sabari, Malarvizhi, and Balasubramanian 2016b).

During FSW and UFSW of AA 7050 (Rui-dong et al. 2011), the S line characteristic is also detected in the SZ of AA 7055 (Wang, Zhao, Yan, et al. 2015). The "S line" is a defect caused by the breaking up of the oxide layer due to insufficient material stirring. Welding with water prevents air oxidation of the plate, resulting in the elimination of the S line fault.

2.11. Summary of Literature Review and Research Gaps

The following are the primary results of the publications reviewed: -

- ✓ Researchers investigate the UFSW in terms of mechanical and microstructure properties on aluminium and some other alloys based on the survey through literature reviews. The majority of researchers came to the conclusion that UFSW, as compared to conventional FSW, can increase strength and microstructure qualities at the joint region.
- ✓ It is observed that UFSW is more suitable to heat-treatable aluminium alloys as it reduces the softening effect.
- ✓ Increased tensile strength, hardness and decreased % elongation were reported by many researchers in SFSW over that of FSW due to the higher cooling rate in SFSW.
- ✓ The key and capital virtue process factors for attaining the greatest tensile and hardness strength during both friction stir welding and SFSW of aluminium and related alloys are rotational speed, traverse speed, axial force, and tool pin profiles.
- ✓ It is observed that the use of diverse parameters yields a variety of outcomes. It is obvious from the types of research studied that traverse speed and axial force magnitudes are dependent on the levels of rotational speed that confer rotational speed on a sound weld. The tool rotational speed is inversely related to the traverse speed and directly proportional to the axial force and dwell time.
- ✓ The majority of the numerical models in the literature were created in ABAQUS utilizing Lagrangian part specification, which has a significant computational cost. The model built utilizing Eulerian material specification decrease computational time significantly.

CHAPTER THREE

MATERIALS AND METHODS

This chapter goes through the materials and instruments that were utilized to weld and test the specimen in detail. The study's experimental flowchart is depicted in the diagram below.

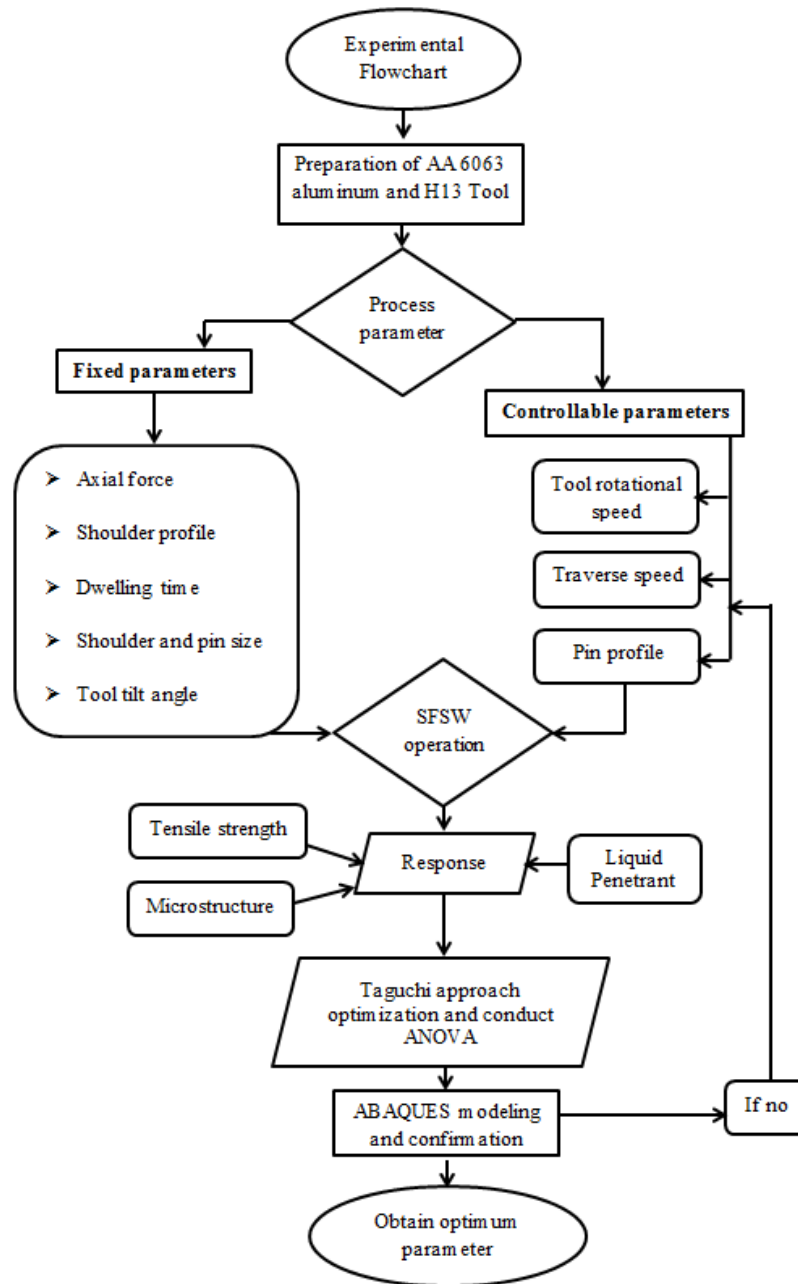


Figure 3. 1 Study framework

3.1. Materials

3.1.1. Tools and Equipment

The holding fixture was designed and manufactured in such a way for easy and good usage. Furthermore, the fixture was made to grip the two aluminium parts that are going to be welded together, preventing them from moving or rotating in any way. A specifically developed 18 mm shoulder diameter with 4.5 mm pin length and 6 mm pin diameter H13 steel tool was used in the study. In addition, the welding tool was driven by a vertical milling machine.

Steel container was created for immersing purposes, allowing the work item to be fastened in and put into the milling machine. The container used measures 40 cm length, 30 cm width and 10 cm height. The container also has a capacity up to 3-liter and can be used to submerge the sample in water at any temperature.



Figure 3. 2 view of sample prior to welding and holding fixture

A thermometer was installed to record the temperature during the welding process and it was situated at some distance from the stir zone.

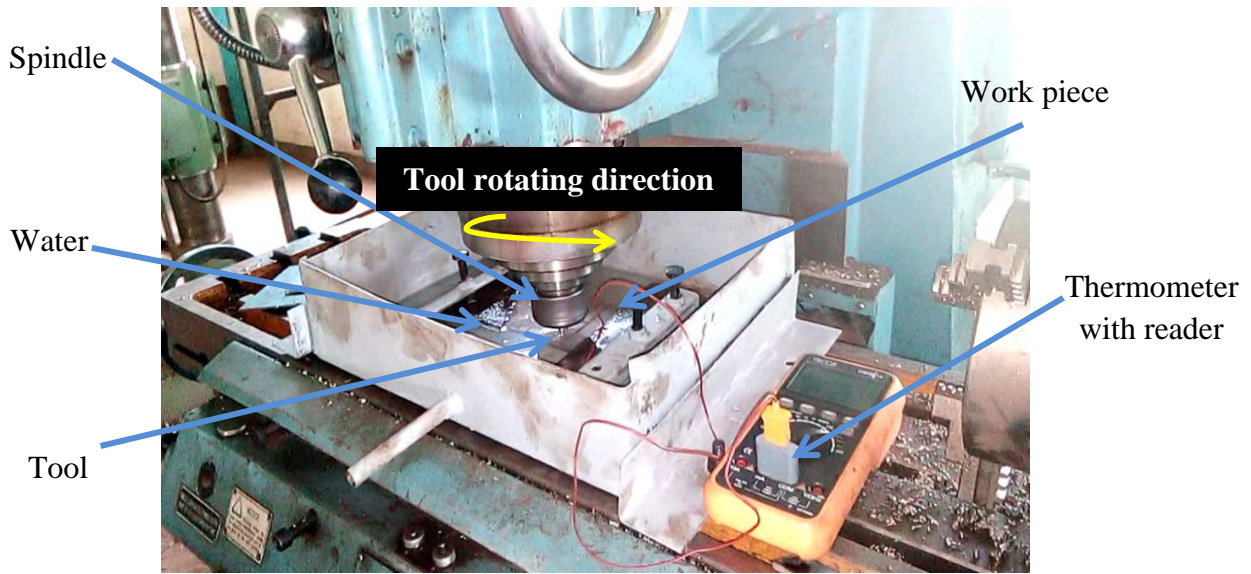


Figure 3. 3 Full setup used in the experimental work

The samples were made of 6063 aluminium alloy with a thickness of 5 mm and dimensions of 120 mm length and 80 mm width. Three different non-consumable tools made of H13-tool steel with shoulder diameter of 18mm, pin diameter 6 mm, and pin length of 5 mm were used to perform the procedures. The fixture was joined with the tank and the samples were clamped on it. Water was poured into the container until it reaches the top surfaces of the samples, and the water temperature was ideal, 30°C during the experiment.

Table 3. 1 Machines used in the study

No_	Machines	Purpose
1.	Heat treatment	To Heat treat the tool
2.	Shear machine	To cut the work piece (aluminium)
3.	Vertical milling machine	To perform the SFSW process
4.	Lathe machine	To prepare the tool
5.	UTM	To perform tensile strength test
6.	Optical microscope	To observe metallographic image
7.	H13 tool	To perform the welding by generating heat during the process and plasticized materials.
8.	Clamp	To hold and fix the work piece with the backing plate during welding.

3.1.2. Aluminium alloy -6063

The Aluminium Association has created a naming method that organizes aluminium alloys based on alloying elements and material qualities, using a four-digit "name" to differentiate them from one another. The first digit of this term denotes a group of alloys divided mostly by alloying components. 6063 aluminium is one of the 6xxx alloys, which add magnesium and silicon to the base aluminium to make it stronger. 6063 aluminium alloy is heat treatable, weldable, corrosion-resistant, and easily produced. Because it includes less copper, which increases corrosion susceptibility, it is more corrosion resistant than 6061 aluminium. AA 6063 aluminium plates and rods are one of the most heat-treatable alloys available. The majority of its applications are in the manufacturing of aluminium furniture, piping, tubing, and window and door frames for buildings.

AA 6063 is used as work piece in the present study. All specimens were cut off at equal dimensions of 101.6 mm length and 80 mm width using shear cutting machine.

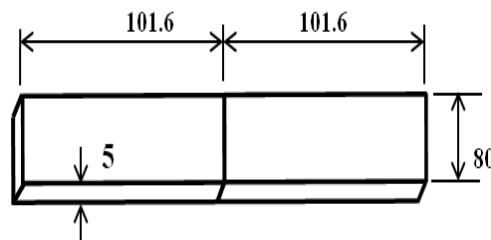


Figure 3. 4 Dimension of aluminium used in the study

The chemical composition of the plate was detected using SPECTROSCOPY machine and the results are summarized and shown in below.

Table 3. 2 Typical composition of Aluminium Al 6063 alloy (Davis 2001)

Chemical Element	Mn	Fe	Mg	Si	Zn	Ti	Cr	Cu	Others	Al
Composition	0.10	0.35	0.45 - 0.9	0.2-0.6	0.10	0.10	0.10	0.10	0.15	Balance

Magnesium silicon, and iron are balancing elements which can hold up to 2% of the total composition of the material. All physical, mechanical and thermal properties of AA 6063 are presented in below tables.

Table 3. 3 Physical Property Aluminium Al 6063 alloy (Kaviyarasan et al. 2020)

Physical Property	Value
Density	2.70 g/cm ³
Poisson's Ratio	0.33
Modulus of Elasticity	69.5 GPa
Electrical Resistivity	0.033 x10 ⁻⁶ Ω .m

Table 3. 4 Mechanical Property Aluminium Al 6063 alloy (Kaviyarasan et al. 2020)

Mechanical Properties	Value
Tensile Strength	186 MPa
Yield Strength	160 MPa
Elongation at break	18-33%
Hardness	25 (HB)
Shear Strength	152 MPa
Young's Modulus	68.9 GPa
Shear Modulus	25.8 GPa

Table 3. 5 Thermal Properties of Al 6063 alloy (Kaviyarasan et al. 2020)

Properties	Value
Thermal expansion	23.4 (10 ⁻⁶ /°C)
Melting Point	622-655 °C
Thermal conductivity	201- 218 W/mK

3.1.3. Welding tool materials

H13 tool steel is classified as a hot working tool steel and the next significant alloying element is chromium material. H13 tool steel offers strong shock and abrasion resistance combined with red hardness, easy machinability, good elevated temperature strength, and a good price compared to others, according to (Said et al. 2015). Furthermore, the tool is ideal and frequently used for welding of comparable and dissimilar aluminium materials with thicknesses ranging from 0.5 to 50 mm, according to previous study. As a result of the aforesaid considerations, the H13 tool steel was chosen as the tool materials in the present study.



Figure 3. 5 H13 tool steel

Each three tools were made of H13 tool steel with different profiles. The tool profile was selected based on the previous studies in which better weld properties were recorded. All mechanical property and chemical composition of H13 tool are listed below.

Table 3. 6 Chemical compositions of H13 tool steel (Said et al. 2015)

Materials	Composition (%)
Chromium, Cr	4.75-5.50
Molybdenum, Mo	1.10-1.75
Silicon, Si	0.8-1.2
Vanadium, V	0.8-1.2
Carbon, C	0.32-0.45
Nickel, Ni	0.3
Copper, Cu	0.25
Manganese, Mn	0.2-0.5
Phosphorus, P	0.03
Sulphur, S	0.03
% Fe	Remaining

Following Iron, chromium and molybdenum are elements which contribute a minimum of 4.75 % and 1.10% respectively to the total composition of H13 tool steel. The least contribution is 0.03% by sulphur and phosphorus.

Table 3. 7 Mechanical properties of H13 tool steel (Said et al. 2015)

No	Properties at 20°C	Mechanical strength, [MPa]
1	Ultimate Tensile Strength	1200-1590
2	Hardness [HRC]	55
3	Yield Strength	1000-1380
4	Modulus of Elasticity	215116.42
5	Reduction of Area	50%
6	Poisson's Ratio	0.27-0.3

The mechanical characteristics of the tools (1200-1500 MPa) are higher than the mechanical qualities of the welding specimen. Therefore, the welding tool is safe to use for joining the specimen without breaking.

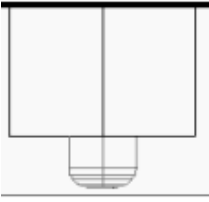
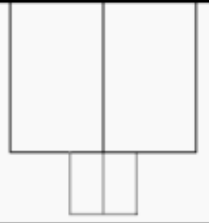
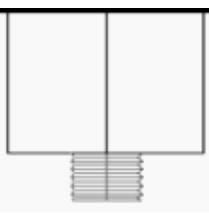
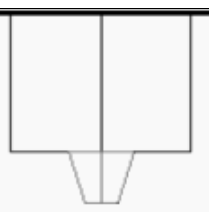

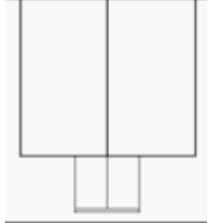
3.1.3.1. H13 tool steel selection criteria

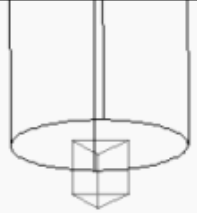
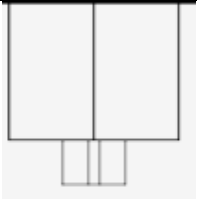
H13 tool steel is a hot working tool steel, and the next important alloying ingredient is chromium material. According to research surveys, H13 tool steel offers excellent shock and abrasion resistance mixed with red hardness, easy machinability, good elevated temperature strength, and a low price when compared to others. Furthermore, the tool is suitable and widely used for welding of comparable and dissimilar aluminum materials with thicknesses ranging from 0.5 to 50 mm. As a result of the aforementioned considerations, H13 tool steel was chosen as the tool material.

3.1.3.2. Determination of tool pin geometry

Three compatible tool geometries were selected among many geometries and characteristics. The effects of different pin geometries on FSW process were analysed according to (Verma, Gupta, and Misra 2016).

Table 3. 8 Characteristics and effects of different pin geometries on FSW process (Verma, Gupta, and Misra 2016).

Tool shapes	Geometry	Characteristics and their effects
	Domed surface pin	<ul style="list-style-type: none"> ✓ Improve the quality of weld and tool life, ✓ Simple in Design.
	Cylindrical pin without thread	<ul style="list-style-type: none"> ✓ Simple in Design, ✓ No pulsating stirring.
	Threaded cylindrical	<ul style="list-style-type: none"> ✓ Ratio of plasticized material from static volume to dynamic volume (ratio of swept volume) is 1.01, ✓ No pulsating stirring, ✓ Compression of the weld zone, ✓ The stirring material moves from the top to bottom of the pin via threads and deposited in the stir zone.
	Tapered cylindrical	<ul style="list-style-type: none"> ✓ Ratio of plasticized material from static volume to dynamic volume (ratio of swept volume) is 1.09 ✓ No pulsating stirring.
	Threaded taper	<ul style="list-style-type: none"> ✓ Extremely uniform particle distribution, ✓ Hardness of the joint has a good correlation with the grain size.
	Square pin	<ul style="list-style-type: none"> ✓ Incompressible material flow, ✓ Ratio of plasticized material from static volume to dynamic volume (ratio of swept volume) is 1.56 ✓ Pulsating stirring, ✓ Higher mechanical strength.

	<p>Triangular pin</p>	<ul style="list-style-type: none"> ✓ It is associated with eccentricity ✓ Incompressible material flow during the process, ✓ Ratio of plasticized material, From static volume to dynamic volume (ratio of swept volume) is 2.35 ✓ Pulsating stirring, ✓ Higher mechanical strength.
	<p>Four flute square</p>	<ul style="list-style-type: none"> ✓ Large Cluster formation in nugget zone ✓ Hardness of the joint has a good correlation with the grain size.

3.1.3.3. Determination of Pin diameter and its length

To control undercut faults during welding, the length of the pin should be less than 0.3 mm of the base material thickness. The maximum outer pin diameter is calculated by $0.8 \times \text{Plate thickness (mm)} + 2.2$, according to a study by (Khalilabad et al. 2016). As a result, used the tool length was determined to be 4.7 mm \approx 4.5 mm, and the pin diameter was calculated to be $0.8 \times (5 \text{ mm}) + 2.2 = 6.2 \text{ mm}$ approximated to \approx 6mm.

3.1.3.4. Determination of Shoulder diameter

Researchers discovered good mechanical properties by utilizing a D/d ratio of 3. In this study, the tool diameter was previously established to be 6 mm; hence 18 mm shoulder diameter was chosen to achieve a D/d ratio of 3.

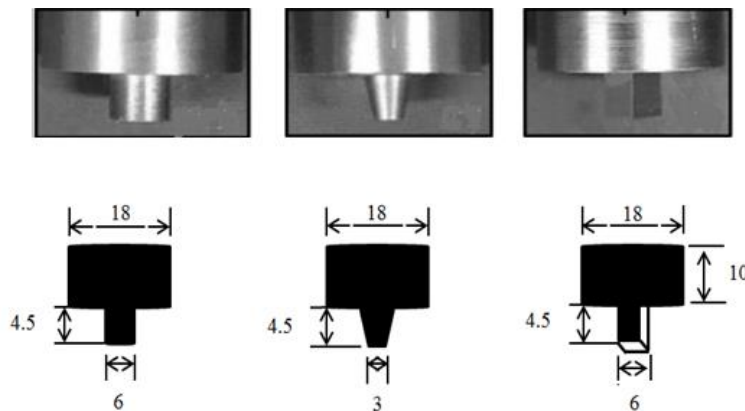


Figure 3. 6 Design of the tools with their dimension in (mm)

Types and shapes of the tool have a major impact on the flow of plasticized material. The tool pin profile's main function is to control the flow of molten material. Three alternative tool pin profiles including straight cylindrical, tapered cylindrical and square pin were used in the study as shown in above figure.

3.2. Experimental Machine and setups

Samples made of 6063 aluminium alloy with a thickness of 5 mm and dimensions of 120 mm length and 80 mm width were used in the study. Non-consumable tool of H13-tool steel with shoulder diameter of 18 mm, pin diameter of 6 mm, and pin length of 4.5 mm was used to perform submerged friction stir welding procedures. The fixture was joined with the tank and the samples were clamped on it. At starting the water outlet was closed and water was poured by coolant hose into the tank until it reaches the top surfaces of the samples. After reaching the top, water outlet will open but still the water flows continuously behind the rotating tool following the weld direction. The water temperature was 30°C during the experiment.

The work piece holder (fixture) was built of steel and a manual metal arc welding machine was used to fuse it together. Using a hexagonal bolt and a C-clamp, the specimen's degree of freedom was restricted in all directions.



Figure 3. 7 Container and work piece holder/fixture

The study was carried out by adjusting the rotational speeds of 900 rpm, 1200 rpm, and 1400 rpm. Axial load of 7 KN and dwelling time of 10 s were constant parameters.

3.2.1. Welding Machine

FSW machine is not available in Ethiopia in any of manufacturing industries. Therefore, vertical milling machine was used as FSW machine in this research.

On a vertical milling machine, the processes of friction stir welding and submerged friction stir welding can both be carried out. As a result, the work piece was appropriately clamped on the machine table and the tool was put on the machine's spindle. A rectangular work pieces were cut by shear cutting machine. The plate was welded under butt joint. H13 tool steel was used to create three tools with three different pin profiles: square, taper, and straight cylindrical. Heat treatment was used to get the best possible hardness. After hardening, the tool material had a hardness value of 52 HRC.



Figure 3. 8 Vertical Milling machine

3.2.2. Experimental Procedures

The study was performed at a greater rotational speed due to the increased heat input required to account for the heat lost in water compared to air. Therefore the process took place at 900, 1200 and 1400 RPM with 15, 30 and 45 mm/min and using three different tool pin shapes namely: straight cylindrical, taper cylindrical and square tool. Water flows from the coolant hose

continuously behind the rotating welding tool in the direction of weld. After completing the process, smaller specimens for tensile testing and microstructure assessment was collected from the welded samples. Specimens were ground and polished with sand paper before microstructure examination. Microstructure observation was examined using optical microscope and tensile test was done using universal testing machine (UTM). In addition to that, liquid penetrant testing was done using cleaner, penetrant and developer.

The joints were sectioned at a 90-degree angle to the welding direction using a wire electrical-discharge cutting machine (WEDM) for tensile and metallographic analysis. The welded specimen's cross-sections were polished with various grits and etched with reagent for metallographic investigation. The tensile specimens were made according to ASTM [E8M-04] international codes.

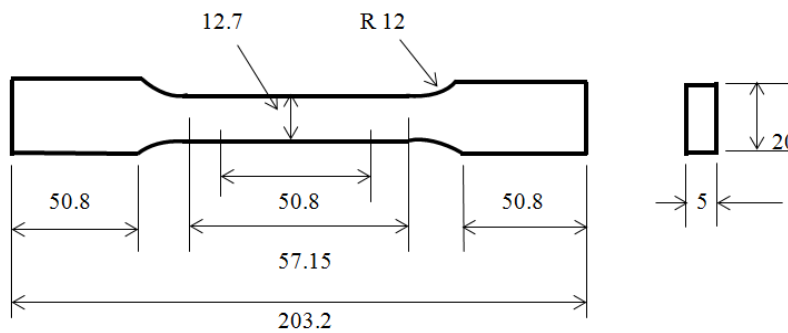


Figure 3. 9 Size of the tensile specimen (ASTM E8-04)

3.3. Inspection and testing

3.3.1. Tensile test

A material's tensile strength is the highest amount of tensile stress it can withstand before failing. A uniaxial load is applied to both ends of the sample during the tests. The specimen's dimensions are (203.2 x 20 x 5) mm. Parent material's tensile test was taken place for comparison.



Figure 3. 10 AA6063 parent material and experimental test specimens

Universal testing equipment (UTM) was used to examine the specimen. The samples were let to break until they reach their full tensile strength. For determining ultimate tensile strength, the stress-strain curve was displayed. The data for the tensile test was obtained immediately from the machine and plotted. The test samples were prepared according to the ASTM E8-04 specimen geometry standard.



Figure 3. 11 Tensile test machine

3.3.2. Liquid penetrant test

It is a method that can be used to detect open-to-surface discontinuities in any non-porous industrial product. In this procedure, a liquid penetrant was applied to the sample surface for a predetermined amount of time. The penetrant that was left in the discontinuity was absorbed by the developer to show the discontinuity's presence as well as its location, size, and type.

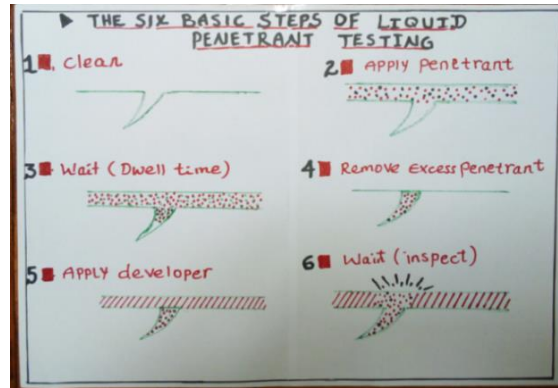


Figure 3. 12 Steps in liquid penetrant testing

First the surface was cleaned by applying cleaner then after cleaning the surface, the penetrant was applied along the welding line for 10 minutes, and then developer was applied over the penetrant. Finally, the weld surfaces were visually checked to determine which process conditions result in crack-free welded junctions.



Figure 3. 13 Cleaner, Penetrant, and Developer

3.3.3. Microstructure

The microstructural morphology consists of the nugget zone, the thermal-mechanical-affected zone (TMAZ), the heat-affected zone (HAZ), and the base-material zone. The microstructures of the samples were observed by optical microscopy. The shapes and grey levels of the microstructure morphology in the cross-section area of the weld are related to the peak temperature experienced in each region.

The specimen preparations of sample to examine microstructure were cutting of specimen, grinding, polishing with different grades (120, 150, 180, 220, 280, 360 400 and 1000 grits) of sand paper, etching and polishing carefully. Water was used for washing and dried by

pressurized compressor. The etchant used to test this microstructural was ethanol. In this study the microscopic images were observed by optical microscopy with Magnification X20 and X50.



Figure 3. 14 Optical microscope

3.4. Determination of parameters with their levels

In order to determine the proper traverse speed, rotational speed, and tool shape for the target material of AA 6063, the levels in the relevant literature are surveyed and their frequencies are chosen. This indicates that the level magnitudes that consistently produce the greater response value are chosen.

3.4.1. Determination of RPM levels

Table 3. 9 RPM with UTS result

Study title	Used material	Rotational speed (RPM)	Optimized RPM	maximum stress result	Reference
Optimization of process parameters of FSW of aluminium alloys (6061) Using Taguchi Method	AA 6061	1000, 1200 and 1400	1200	151 MPa	(Kumar, 2016)
Influence of Friction Stir Welding process and tool parameters on strength properties of AA7075-T6 aluminium alloy joints	AA7075-T6	900, 1200, 1400, 1600 and 1800	1400	T.S. = 372 MPa H.S. = 203 Hv	(Rajakumar et al., 2011)

Effect of Friction Stir Welding parameters on the microstructure and mechanical properties of AA2024-t4 aluminium alloy	AA 2024-T4	500, 700, 900, 1400 and 1800	900	T.S. = 360 MPa H.S. = 100.8 Hv	(Abdel-Wahab El Morsy, 2018)
Investigation of submerged FSW of marine-grade aluminium alloy	AA 5083	800, 1000 and 1200	1000		(Emad Eldin Mohammed Kishta 2014)
Optimization of process parameters in friction stir welding of al 6063	AA 6063	1000 and 1400	1400	T.S. = 92 MPa	(C.DEVANATHAN, 2013)

Based on the preceding table and additional literature searches, the current study's RPM parameters are 900, 1200, and 1400 rpm.

3.4.2. Determination of traverse speed levels

Table 3. 10 Traverse speed with UTS

Study title	Used material	Traverse speed, [mm/min]	Optimized TS [mm/min]	maximum stress result	Reference
Effect of FSW parameters on microstructure and mechanical properties of AA2024-T4 aluminium alloy	AA 2024-T4	11, 18, 28, 35 and 45	35	T.S. = 360 MPa	(Abdel-Wahab El Morsy, 2018)
Effect of tool rotational speed on mechanical properties of	AA 5083	40	40	T.S. = 203.5 MPa	(Prabha et al., 2018)
Experimental and Parametric Analysing of FSW for AA-6061	AA 6061	15, 25 and 35	15	T.S = 293 MPa	(Tolcha and Melaku 2020)
process parameter optimization for FSW of RDE-40 aluminium alloy using Taguchi technique	RDE-40 AA	22, 45 and 75	45	T.S. = 264.3MPa	(Lakshminarayanan and Balasubramanian, 2008)

Even though the magnitude and range of intervals for each traverse speed are different, three levels of traverse speed of 15, 30, and 45 mm/min were chosen depending on the determined

RPM. The Levels interval range was equal in magnitude differences. As a result, the aforesaid level of difference is divided by 15 intervals.

3.5. Optimization and Design of Experiments

The welding engineer tried to select welding parameters based on prior experience when determining the appropriate welding procedure for a given set of properties, but a number of experimental trials may be carried out, eventually leading to the definition of the optimal welding parameters. This procedure takes longer and is more costly (Soundararajan, Zekovic, and Kovacevic 2005). There are many ways and procedures for determining process parameters; however the method shown below (Taguchi method) is suitable and commonly utilized to explore the process parameters optimization of the welding process.

3.5.1. Taguchi method

The Taguchi approach relies on the optimization of process parameters to achieve excellent quality without raising costs. It uses a statistical measure of performance termed signal-to-noise (S/N) to analyse the findings. This S/N ratio is used to determine which control levels are ideal for dealing with noise (Dhas and Dhas 2012). The influence of three parameters with three levels each was evaluated in the study.

3.5.2. Selection of Orthogonal array

The minimum number of experiments to be conducted in the overall experiment based on the formula below.

$$N = Lf \quad 3.1$$

Where: N = No. of experiments, f =Number of parameters and L=Number of levels.

The mixed L9 orthogonal array was an appropriate design for the characteristics and levels. This orthogonal array was used for nine experimental runs. In the layout of the L9 orthogonal array, the selected process parameter and levels are shown in the table below. Selected L9 orthogonal array has 8 degree of freedom for 3 levels and 3 factors; DOF is equal to 2^3 .

Table 3. 11 Process parameters and their levels

Exp No.	Rotational speed (Rpm)	Traverse Speed (mm/min)	Tool Shape
1.	900	15	str.cyl
2.	900	30	tap.cyl
3.	900	45	square
4.	1200	15	tap.cyl
5.	1200	30	square
6.	1200	45	str.cyl
7.	1400	15	square
8.	1400	30	str.cyl
9.	1400	45	tap.cyl

3.5.3. ANOVA Approach

ANOVA can be used to determine which process factors are statistically significant and which parameter affects the study's response. It was employed by various researchers to find parameters that contributed to the study's response. As a result, the most important process parameters that significantly improved the study's response were examined and determined in this study.

A fishbone diagram was used to identify the fundamental causes of the specified parameters. Cause and effect diagram of study's parameters influencing on submerged friction stir welding joint strength was drawn. Tool rotation speed, traverse speed, and tool pin profile were used as variable parameters and axial force, tool material, dwelling time and plunger depth were the study's fixed parameters.

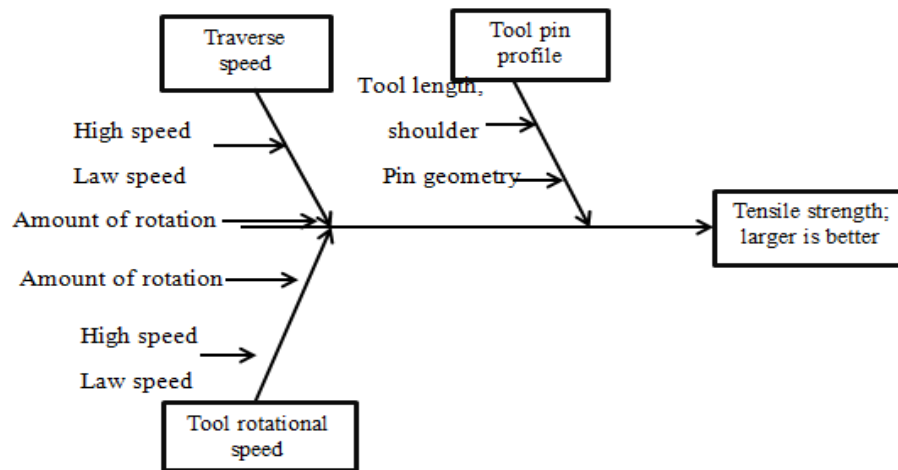


Figure 3. 15 Cause and effect diagram of parameters influencing SFSW joint strength

3.6. Heat generation at tool-work Piece Interface

The heat created by the shoulder is well recognized to play a substantial role in overall heat generation, and the interaction between the shoulder and the workpiece can have a significant impact on the temperature field. The plunge force is also frequently utilized in heat generation calculations. The shoulder's diameter has an impact on how much heat it produces; as the shoulder's diameter increases, so does the amount of heat produced.

The heat required to join the materials ranges from 80 to 90% of the melting point. The heat generated by friction between the work pieces and tool can be calculated (Jain, Pal, and Singh 2017).

$$qf = \frac{4}{3} \pi^2 \mu PNR^3 \quad 3.2$$

Where μ is the coefficient of friction, P is the traction, N is the rotational speed, and R is the shoulder radius. When a rotating tool moves over a stationary work piece, friction is produced. This friction work, which can be converted to heat, is caused by the velocity differential between the dynamic spinning tool and the stationary work material. In this study, analytical and ABAQUS software were used to calculate the temperature generations for three different tool profiles.

The analytical expression for heat generation is in the form of heat flux, and the total heat flux is as follows (Hilgert et al. 2011):

$$q_{total} = q_{friction} + q_{plastic} = \omega r \tau_{yield}(T) \quad 3.3$$

Where r is the distance from the heat source centre, and $\tau_{yield}(T)$ is the shear yield stress, which is equal to $\sigma(T)/\sqrt{3}$ according to the von-Mises yield criterion.

The quantity of heat created by friction and plastic deformation is determined by the contact situation between the tool and the work piece. This shows that the pin's shoulder, side surface, and tip generate heat.

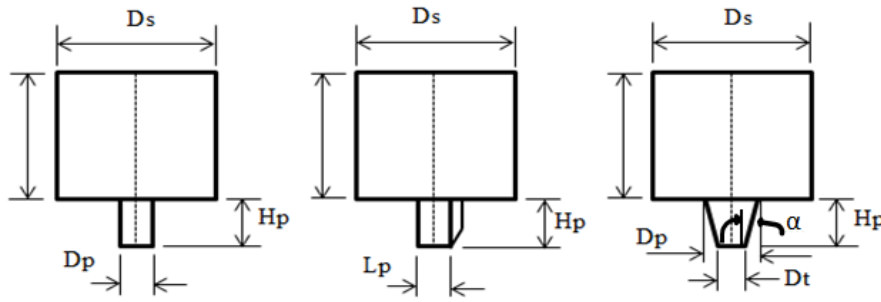


Figure 3.16 Tool geometries: straight cylindrical, square and taper cylindrical tool

By calculating the integration equation throughout the shoulder area from R_p to R_{sh} , the shoulder heat generation, Q_1 , is computed (H Schmidt, Hattel, and Wert 2003):

$$Q_1 = \int_0^{2\pi} \int_{R_p}^{R_{sh}} \omega \tau_c r^2 (1 + \tan \alpha) dr d\theta = \frac{2}{3} \pi \tau_c \omega (R_{sh}^3 - R_p^3) (1 + \tan \alpha) \quad 3.4$$

Where, τ_c = is contact shear stress and α = tilt angle/orientation = $\frac{R_p - R_t}{H_p}$

The probe generates two types of heat: Q_2 from the side surface and Q_3 from the tip surface. The following are the results of heat generation on the probe side and probe tip area:

$$Q_2 = \int_0^{2\pi} \int_0^{H_{pro}} \omega \tau_c R_p^2 dz d\theta = 2\pi \tau_c \omega R_p^2 H_p \quad 3.5$$

$$Q_3 = \int_0^{2\pi} \int_0^{R_p} \omega \tau_c r^2 dr d\theta = \frac{2}{3} \pi \tau_c \omega R_p^3 \quad 3.6$$

The Overall heat generation estimate Q_{total} is calculated by combining the three contributions.

$$Q_{\text{total}} = Q_1 + Q_2 + Q_3 = \frac{2}{3}\pi\tau_c \omega [(R_{\text{sh}}^3 - R_{\text{p}}^3) (1+\tan \alpha) + R_{\text{p}}^3 + 3R_{\text{p}}^2 H_{\text{p}}] \quad 3.7$$

3.6.1. Contact shear stress

When a work piece deforms, the revolving layer of softened material travels around the welding tool. Only if the welding tool's stresses generate tangential strains greater than the shear yield strength is this possible. The boundary value of such tangential shear (contact) stress is according to von Misses yield criteria in uniaxial tension and pure shear (H Schmidt, Hattel, and Wert 2003):

$$\tau_c (T) = \tau_{\text{yield}}(T, \epsilon) = \sigma_{\text{yield}}(T, \epsilon) / \sqrt{3} \quad 3.8$$

The mechanisms that create contact shear stress differ depending on whether there is a sliding or sticking state. If the sticking interface condition is assumed, the matrix closest to the tool surface adheres to it. The yield stress is not affected by pressure, but it is affected by temperature. An isothermal interface is considered when the same shear yield stress is applied to the whole interface. The following phrase is based on the sticking condition:

$$Q_{\text{sticking}} = \frac{2}{3}\pi \frac{\sigma_{\text{yield}}}{\sqrt{3}} \omega [(R_{\text{sh}}^3 - R_{\text{p}}^3) (1+\tan \alpha) + R_{\text{p}}^3 + 3R_{\text{p}}^2 H_{\text{p}}] \quad 3.9$$

The total heat generation for the sliding conditions when the tool surface and weld material are sliding toward each other is provided by:

$$Q_{\text{sliding}} = \frac{2}{3}\pi\mu p \omega [(R_{\text{sh}}^3 - R_{\text{p}}^3) (1+\tan \alpha) + R_{\text{p}}^3 + 3R_{\text{p}}^2 H_{\text{p}}] \quad 3.10$$

3.7. FE modelling

The FE modelling aims to provide a better understanding of the process through more detailed analysis than the experimental studies. In numerical analysis, FEM is most typically used to obtain approximate solutions to a wide range of engineering issues.

The experimental approach to optimization wastes a lot of resources and takes a long time. To overcome these obstacles, finite element simulation is used to find the best solution based on a

specific set of process parameters. In this study, ABAQUS is used to do finite element analysis, specifically using the Coupled Eulerian-Lagrangian (CEL) method. The CEL approach provides a lot of advantages when it comes to defect prediction in SFSW and choosing the best process parameters. It also aids in the reduction of simulation duration, hence making SFSW finite element simulations safer by removing mesh distortion caused by high deformation.

Numerical modelling can help to fully comprehend specific aspects of a process, such as strain evolution and material flow. Furthermore, by comparing numerical findings to experimental results, the numerical model may be used to forecast changes in outcomes owing to changes in input parameters, saving time and money in the lab. However, numerical modelling in SFSW is problematic since the process requires water as an external parameter; however, in this study, it was accomplished by lowering/minimizing the temperature in the boundary condition.

The ABAQUS program includes a wide range of finite element analysis capabilities, from simple linear static analysis to complicated nonlinear transient dynamic analysis. The thermal and mechanical responses of the material during the submerged friction stir welding process are investigated using finite element simulations. To validate the experimental welding temperature, a transient thermal solver workbench is used in the study. Geometry for simulation purposes is drawn in ABAQUS design modeller based on the experimental setup dimensions.

The geometry of the three tools, namely the square pin tool, the straight cylindrical pin, and the taper cylindrical pin, all with a flat shoulder, was considered. The effects of the various pin profile geometries on the joint quality were investigated.

During the submerged phase, the current FE model accounts for two types of heat generation. Heat generation owing to plastic deformation, r^{pl} , and heat generation due to friction, q , are all examples of friction stir processes. ABAQUS/Explicit utilizes the following equation for the heat flux density to calculate the heat created by friction (Abaqus 6.11 2011):

$$q = q_k + q_r - f q_g \quad 3.11$$

Where q_k is the heat flux due to conduction, q_r is the heat flux due to radiation, f is the fraction of heat generated into the surface and q_g is the heat flux produced by the interface element due to frictional heat generation. The heat flux due to friction is:

$$q_k = k\Delta T \quad 3.12$$

Where ΔT is the difference in temperature between the two surfaces and k is the heat transfer coefficient. The contact pressure, over-closure, and average temperature at the contact site all affect the heat transfer coefficient. The following relation is used to calculate the heat flow caused by radiation.

$$q_r = F[(T_1 - T^Z)^4 - (T_2 - T^Z)^4] \quad 3.13$$

Where T_1 and T_2 are the temperatures on surfaces 1 and 2, respectively, and F is the gap radiation constant. T^Z is the temperature scale's absolute zero. Finally, the heat flow resulting from the formation of frictional heat is provided as follows:

$$q_g = \eta \tau \frac{\Delta s}{\Delta t} \quad 3.14$$

Where Δs is the incremental slip, Δt is the time step, τ is the frictional stress, and η is the heat fraction ABAQUS/Explicit applies the Galerkin method to solve the set of equation for finding the total heat generated due to friction.

As for the heat generation due to plastic deformation, ABAQUS/Explicit assumes that the plastic work caused by the accumulation of plastic strains converts into heat which, in turn, increases the heat flux per unit volume, r^{pl} , as follows:

$$r^{pl} = \beta \boldsymbol{\sigma} : \dot{\boldsymbol{\epsilon}}^{pl}, \quad 3.15$$

Where β is the inelastic heat fraction which represent the percentage of the plastic work that is converted into heat inside the material, $\boldsymbol{\sigma}$ is the stress tensor and $\dot{\boldsymbol{\epsilon}}^{pl}$ is the plastic strain increment tensor. The notation “:” is the double dot product of the two matrices which results in a scalar.

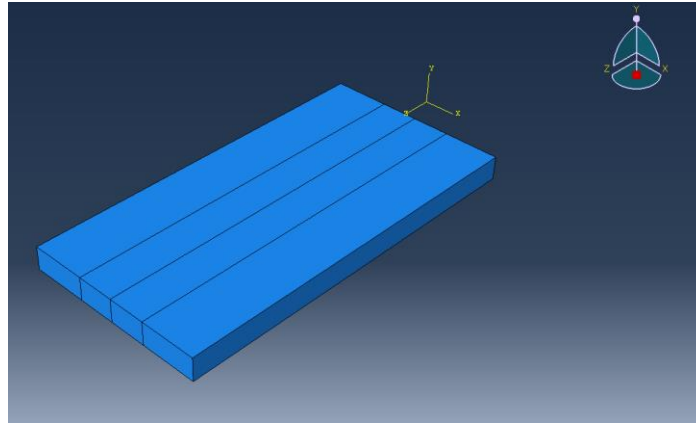


Figure 3. 17 3-D modelling of the Aluminium plate

Frictional heat generation and plastic heat generation calculations demonstrate that the friction between the tool shoulder and the work piece generates the majority of the heat.

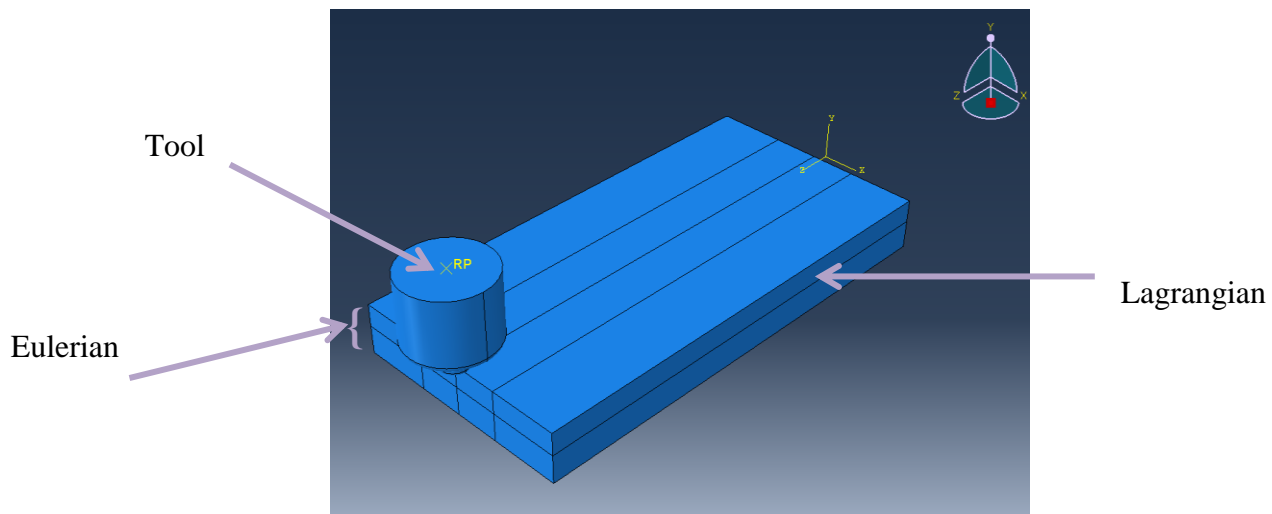


Figure 3. 18 Eulerian- Lagrangian assembly

3.7.1 Material definition

The rotating tool was built of extremely high-strength steel and was defined in FE simulations using the Lagrangian formulation. A tool steel had a specific heat of 0.46 KJ/Kg^*K , a young's modulus of 215 GPa and a thermal conductivity of 28.6 w/m^*k . The plate was manufactured of 6063 aluminium alloy, which has a density of $2.7 \times 10^{-6} \text{ Kg/mm}^3$ and a modulus of elasticity of 70 GPa . It has a thermal conductivity of 200 W/m^*k , with a specific heat of 0.90 KJ/Kg^*K . The

Johnson-Cook material model in ABAQUS software was used to define the thermo-viscoplastic behaviour of the aluminium alloy.

The Backward Euler approach is used as an integration tool to solve non-linear equations using the Newton-Raphson technique. The Johnson-Cook (JC) plasticity and dynamic failure models, which are already incorporated in ABAQUS/Explicit, are used to estimate the material's dynamic flow stress as well as the damage evolution during plastic deformation. The JC dynamic flow stress is given by the following relation (Abaqus 6.11 2011):

$$\sigma = [A+B(\dot{\epsilon}^{pl})^n] [1+ C \ln(\frac{\dot{\epsilon}}{\dot{\epsilon}_0})] (1 - (\frac{T-T_{ref}}{T_m-T_{ref}})^m) \quad 3.16$$

Where A is static yield strength, B is the strain hardening coefficient, $\dot{\epsilon}^{pl}$ is the equivalent plastic strain, n is the strain hardening exponent, C is the strain rate sensitivity factor, $\dot{\epsilon}_0$ is the reference strain rate, T is the temperature, T_{ref} is the reference room temperature, T_m is the melting temperature and m is the thermal sensitivity parameter. The Johnson-Cook plasticity parameters are summarized as:

Table 3. 12 Johnson-Cook parameters for plasticity of AA6063

Plasticity Parameters					
A(MPa)	B(MPa)	C	m	n	$T_m(^{\circ}C)$
11182	24140	0.012	1.003	0.415	655

3.7.2 Mesh description

A total of 4500 elements were used to model the welding plate utilizing 8-node 3D solid elements. To avoid any element distortions during the process, the Eulerian Lagrangian (EL) meshing technique was used. EL meshing is especially critical for big deformation modeling. A percentage of material is specified to fill each element when employing Eulerian elements. If the elements are set to 100 percent material, there will be no area for the material to move about in the elements during deformation, resulting in distortion. Setting the elements to less than 100 percent material, on the other hand, reduces the quantity of material per element and in the entire portion, resulting in voids between the pieces, rendering the model unnatural. The EL approach allows the elements to begin with 100 percent material and gradually reduce the proportion of material per element as the process progresses, allowing the material to stir without distortions or

false voids. Initially, a mesh sensitivity analysis was performed to determine the best element size for accurately simulating the FSW process at a low computational cost.

The type and number of elements are determined by the level of precision and computational power necessary. Smaller mesh sizes take longer to compute, but coarser elements are less accurate. This debate was resolved by determining the optimal mesh size. To begin, a coarse mesh is used and the outcome is recorded. Second, a medium-mesh is utilized, and the temperature result is recorded, and so on, until the temperature result is nearly equal to the previous one.

A fine mesh was utilized near the work piece-tool interaction, when the temperature began to migrate to the other side of the work piece. Around tool interaction, the Eulerian half was meshed with a fine element size of 0.2 and a coarser mesh of 0.5 on the other side. Numerical computation was modelled when the concept had been finalized. The simulation was then carried out using finite element modelling. The tool was mesh in a Tet element shape with a global size of approximately 0.5.

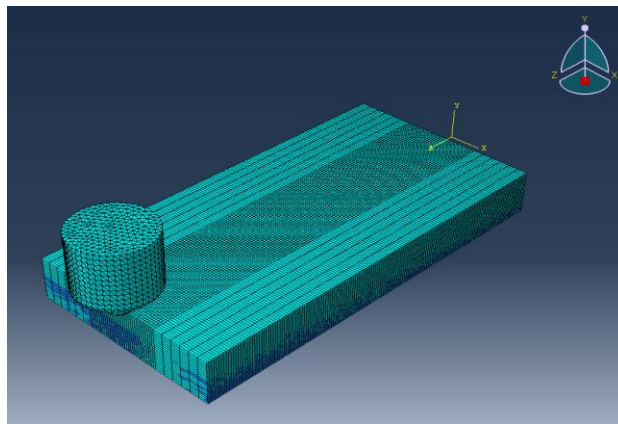


Figure 3. 19 Assembly mesh model

CHAPTER FOUR

RESULTS AND DISCUSSION

4.1. Introduction

The overall results of the tests employing the Taguchi method are presented in this chapter. The goal of the experiment was to determine the optimal tensile strength and microstructure.

The analysis of variance (ANOVA) is the statistical method most usually used to determine the percent contribution of each parameter against a specified level of confidence in the findings of experiments. The optimization of UFSW parameters on selected quality attributes has been explored using plots of the main effects based on the experimental data. S/N data analysis was used to determine the best setting for each of the quality criteria.

4.2. Experimental results

4.2.1. Tensile strength result

The tensile strength of 6063 AA material was conducted using various process parameters, and the response was recorded to draw stress strain curve.

Table 4. 1 Experimental result

No	Rpm	Speed (mm/min)	Tool Shape	UTS(MPa)
1.	900	15	str.cyl	113
2.	900	30	tap.cyl	96
3.	900	45	square	85
4.	1200	15	tap.cyl	71
5.	1200	30	square	116
6.	1200	45	str.cyl	57
7.	1400	15	square	102
8.	1400	30	str.cyl	151
9.	1400	45	tap.cyl	129
10	Parent material			163

The maximum tensile strength of a material is the highest stress that it can withstand before failure or fracture when stretched or pulled. The tensile test was carried out on UTS machine to determine the mechanical properties of the specimens. The information gathered was utilized to create stress strain curve that were used to determine mechanical parameters such as yield strength, tensile strength, and ductility.

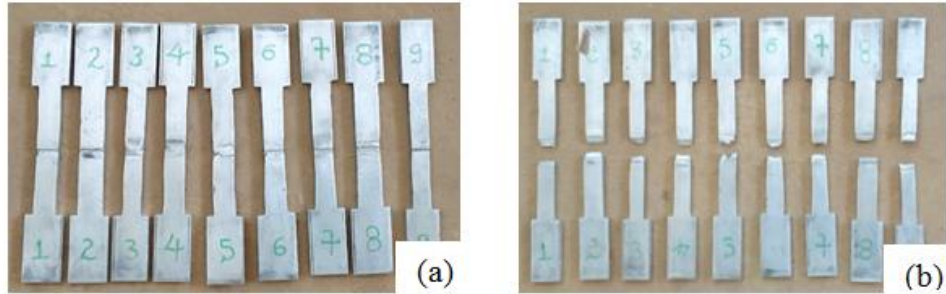


Figure 4. 1 (a) before tensile test; (b) after tensile test

The breaking takes place at the weld joint. This shows that the weld strength at weld zone was slightly lower than that of other area. But the result shows that the maximum tensile strength in MPa of the optimized sample approaches to the parent materials result.

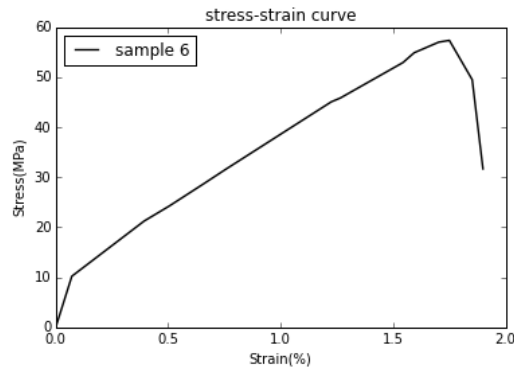


Figure 4. 2 Stress-elongation curve for 1200 RPM, 45mm/min Ts and straight cylindrical tool

The least tensile property was recorded in this sample resulting 57 Mpa. This was because of inappropriate stirring and high feed.

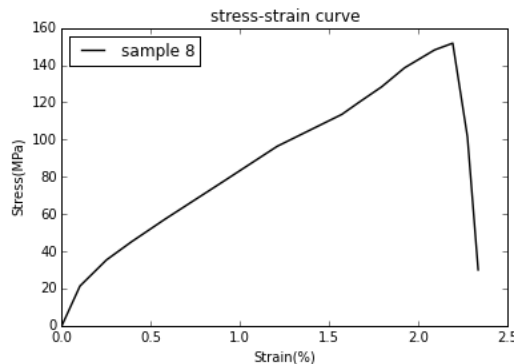


Figure 4. 3 stress-elongation curve for 1400 RPM, 30mm/min Ts and straight cylindrical tool

The maximum tensile strength, which is nearly approximate to that of parent material was measured during the above experiment. Because high tool rotational speed and comparatively

low traverse speed combined with cylindrical tool profile, the tensile result recorded 151MPa. And the parent material's tensile result was 163MPa.

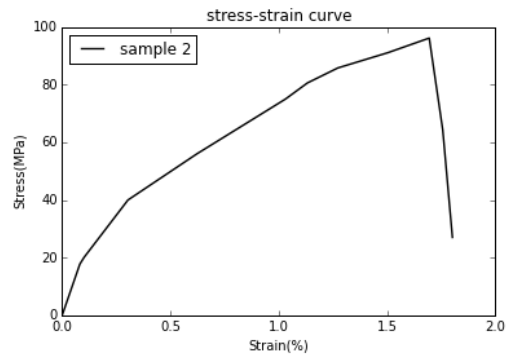


Figure 4. 4 Stress-elongation curve for 900 RPM, 30mm/min Ts and taper cylindrical Straight cylindrical pin profile tool with a rotating speed of 1400 rpm and a traverse speed of 30 mm/min produced a maximum tensile strength of 151 MPa. And the minimum UTS was recorded at rotational speed of 1200 rpm, tapered cylindrical tool pin profile and 45 mm/min TS, resulting 57 MPa. The lower traverse speed and greater rotating speed create appropriate heat for connecting the base metal.

4.2.2. Liquid penetrant test result

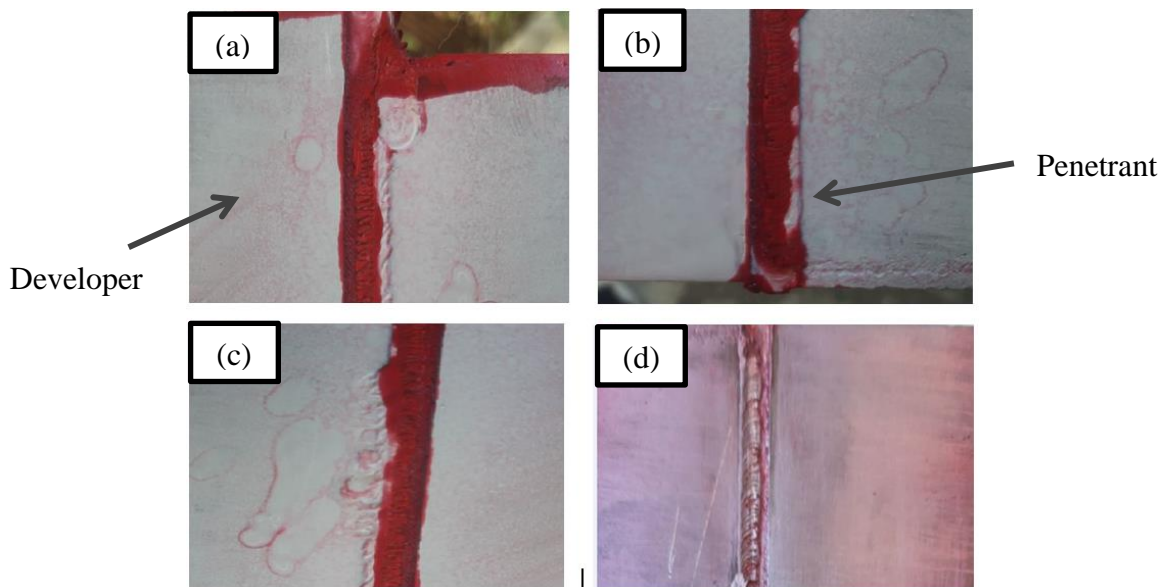


Figure 4. 5 Liquid penetrant test results: (a) 900 RPM, 15mm/min, str. cyl; (b) 1200 RPM, 15mm/min, taper cyl; (c) 1400 RPM, 15mm/min, square tool and (d) after cleaning.

The LPT was done to all nine samples. In trials 2, the test finding demonstrated that there is an evident discontinuity along the weld joint. In addition, in experiments 3 and 7, there is a little spot discontinuity along the joint. This means, the joints were discovered to be more defective than the others. The remaining experiments have a defect-free joint. All of the weld joints had surface cracks at the start and end of the joint. The higher rotational speed provides defect-free joints as a result of the increased heat input and friction.

4.2.3. Microstructure observation result

The specimen preparations of sample to examine microstructure were cutting, grinding, polishing with different grades (120, 150, 180,220, 280, 360 400 and 1000 grits) of sand paper, etching. Then after polishing carefully, it was washed by water and dried by pressurized compressor. The etchant used to test this microstructural was ethanol. The microstructure was observed by using optical microscopy with Magnification X20 and X50. The test was performed for all of 9 samples and the results were collected.

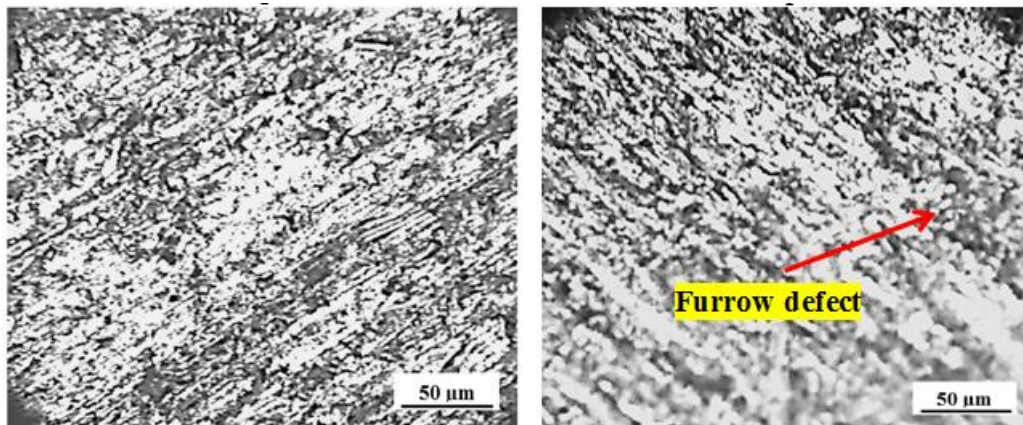


Figure 4. 6 microstructure observation for: (a) 1200 RPM, 45mm/min, straight cylindrical pin; (b) 1400RPM, 30mm/min, straight cylindrical pin.

The result shows that micrographs of the microstructure along the centre of weld have fine grains. Metallographic image was taken along the thickness of the sample. As a result 1200 RPM, 45mm/min, straight cylindrical pin and 1400RPM, 30mm/min, straight cylindrical pin combination shows fine grain compared to the rest. This shows that straight cylindrical pin can provide fine grain with fewer defects than taper cylindrical and square pin.

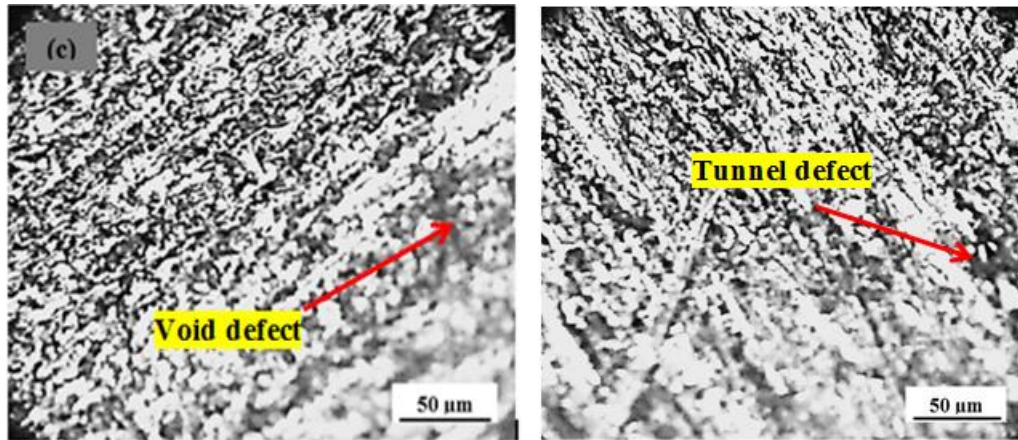


Figure 4. 7 microstructure observation for: (a) 1200 RPM, 30mm/min, square pin; (b) 1400RPM, 15mm/min, square pin.

The observation shows square pin provided poor grain compared to straight cylindrical but the result is better in grain size with less defect than samples conducted using taper cylindrical pin. It might be due to better stirring because of its sharp edge in the weld zone.

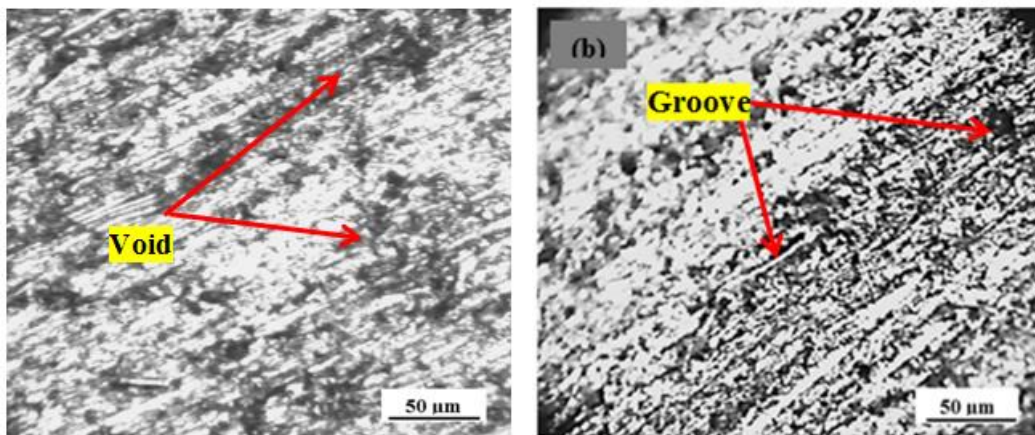


Figure 4. 8 microstructure observation for: (a) 1400 RPM, 45mm/min, taper cylindrical pin; (b) 1200RPM, 15mm/min, taper cylindrical pin.

As a result of taper cylindrical pin, the microstructure observation for 1400 RPM, 45mm/min, taper cylindrical pin and 1200RPM, 15mm/min, taper cylindrical pin combination provided poor grain with some void and grooves respectively. Finally we can say that straight cylindrical pin is better in providing fine grain followed by taper pin.

4.3. Effect of welding parameters on the temperature profiles

The temperature increment was directly proportional to the axial force, tool shape, dwell time, and tool rotating speed. When the values of the above-mentioned parameters were increased, the temperature increased as well, while the traversal speed decreased. The influence of axial force is due to the shoulder forging onto the aluminium sheet surface, which raises the peak temperature. Because of their design and extensive surface area contact with the base metal, straight cylindrical and square tool impart higher heat temperatures than taper cylindrical tool. Rotational speed has a proportionate effect on temperature. The relative velocity between the tool and the aluminium sheet is high at higher rotational speeds. As a result, the heat generation rate and peak temperature are high. Under all processing circumstances, the advancing side of the sheet acquired slightly higher temperatures than the retreating side, demonstrating the asymmetric nature of temperature distribution throughout the welding process. 10 second dwelling time was taken during the operation to each experiment.

Table 4. 2 Relation between parameters and temperature





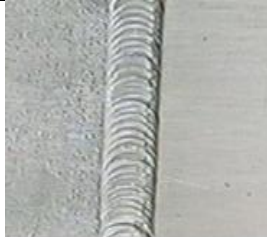
Exp No	Rpm	Travel Speed (mm/min)	Tool Shape	Peak Temp(⁰ C)
1.	900	15	str.cyl	307
2.	900	30	tap.cyl	267
3.	900	45	square	309
4.	1200	15	tap.cyl	327
5.	1200	30	square	321
6.	1200	45	str.cyl	334
7.	1400	15	square	348
8.	1400	30	str.cyl	357
9.	1400	45	tap.cyl	341



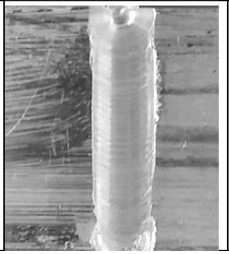

To summarize, increasing the rotational speed will create severe plastic deformation due to the high stirring process, which will result in an increase in temperature. As a result, temperature is proportional to both rotational and axial forces, as well as inversely proportional to traverse speed.

4.4. Effect of welding parameters on the joint quality

The influence of welding parameters on the target material's joint strength is shown in the table below.

Table 4. 3 Effect of weld joints

No.	Weld Joint	Weld Parameters	UTS(MPa)	Defect observation
1		900 Rpm, 15mm/min, straight cylindrical pin	113	Flash defect in retreating side
2		900 Rpm, 30mm/min, taper cylindrical pin	96	Cavity and flash defect due to low RPM
3		900 Rpm, 45mm/min, square pin	85	Flash defect in both sides
4		1200 Rpm, 15mm/min, taper cylindrical pin	71	Defect free joint
5		1200 Rpm, 30mm/min, square pin	116	Defect free joint

6		1200 Rpm, 45mm/min, straight cylindrical pin	57	Flash defect in advancing side
7		1400 Rpm, 15mm/min, square pin	102	Void flow defect
8		1400 Rpm, 30mm/min, straight cylindrical pin	151	Defect free joint
9		1400 Rpm, 45mm/min, taper cylindrical pin	129	Flash defect in advancing side

On the stir zone, Samples 2 and 7 have some cavity and void flaws respectively. Samples 1, 3 and 6 on the other hand, contain flash faults on both the advancing and retreating sides. The remaining experiments have relatively defect-free weld joints. To summarize, due to adequate heat development during the stirring process, rotating speeds of 1200 and 1400 rpm with a combination of 15 and 30 mm/min provide defect-free connections.

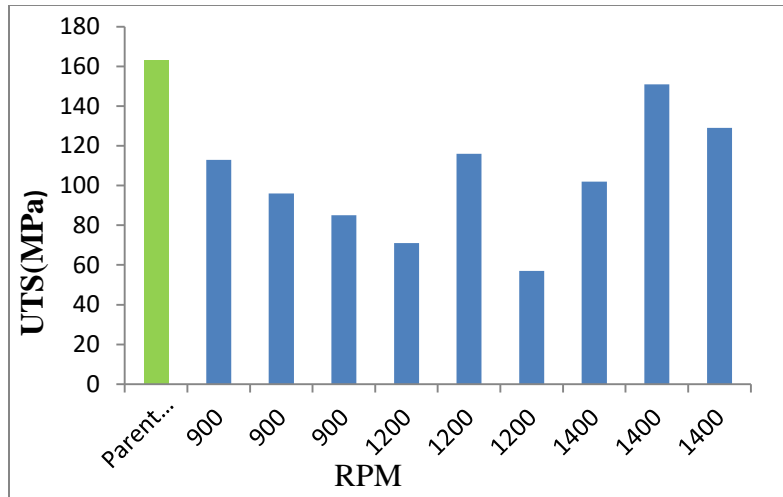


Figure 4. 9 UTS vs RPM graph

The graph shows that tensile strength slightly decreased from 900 RPM to 1200 RPM except for 1200 RPM, 30mm/min traverse speed and it increased from 1200 RPM to 1400 RPM. Therefore increasing the tool rotational speed from 1200 to 1400 RPM will increase the welding temperature and also tensile response.

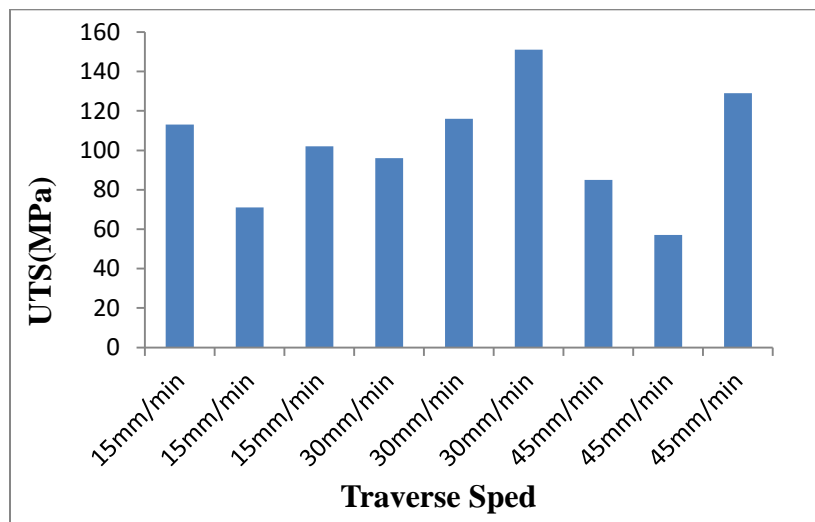


Figure 4. 10 UTS vs Traverse Speed graph

The graph shows that operation performed by 30mm/min traverse speed comparatively provided better UTS value than the rest due to its optimum weld operation.

4.5. FE Result and Validation

ABAQUS software was used to simulate the welding process, which included a shoulder diameter model moving heat source. The current FE model was validated using experimental data from an SFSW sample under similar conditions. The peak temperatures attained at different rotational speeds and the temperature difference between the advancing and retreating sides are among the comparisons between the experimental results and the current numerical analysis. To finish the simulation, transient thermal analysis was employed to simulate the temperature distribution curves.

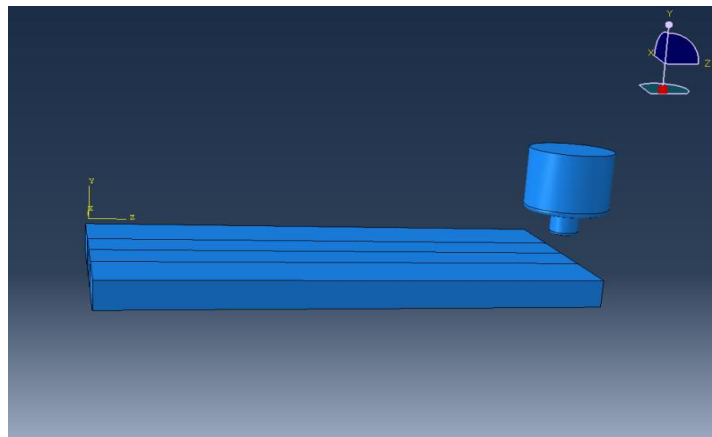


Figure 4. 11 Geometry of the aluminium plate and tool

Experimental findings for an SFSW sample under similar conditions were used to validate the FE model. The peak temperatures attained at various rotational speeds, as well as the difference in temperatures between the advancing and retreating sides are included in the comparison between the experimental results and the current numerical analysis.

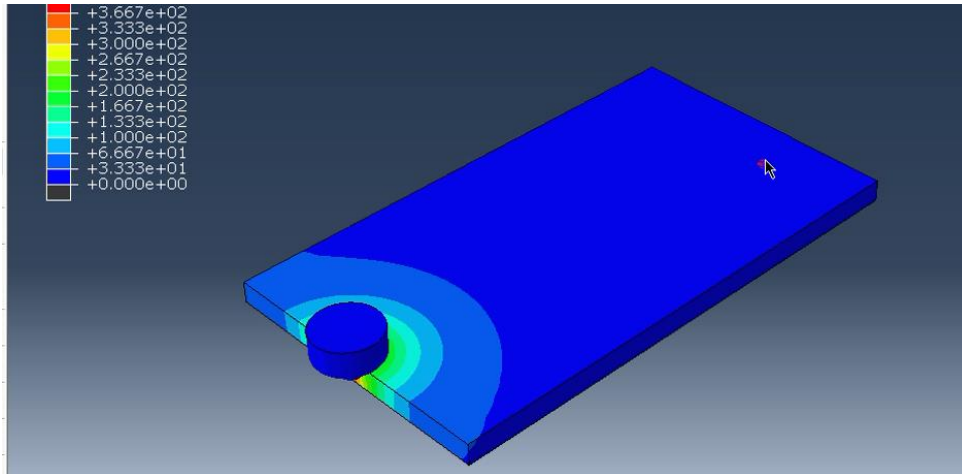


Figure 4. 12 Temperature contour at the beginning

The FE model was performed by three distinct speeds: 900, 1200, and 1400 revolutions per minute. The resulting peak temperatures and thermal profiles observed at these three speeds were compared to the experimental data. At three different rotational speeds, the FE model accurately predicted the temperature profiles of the friction stir process.

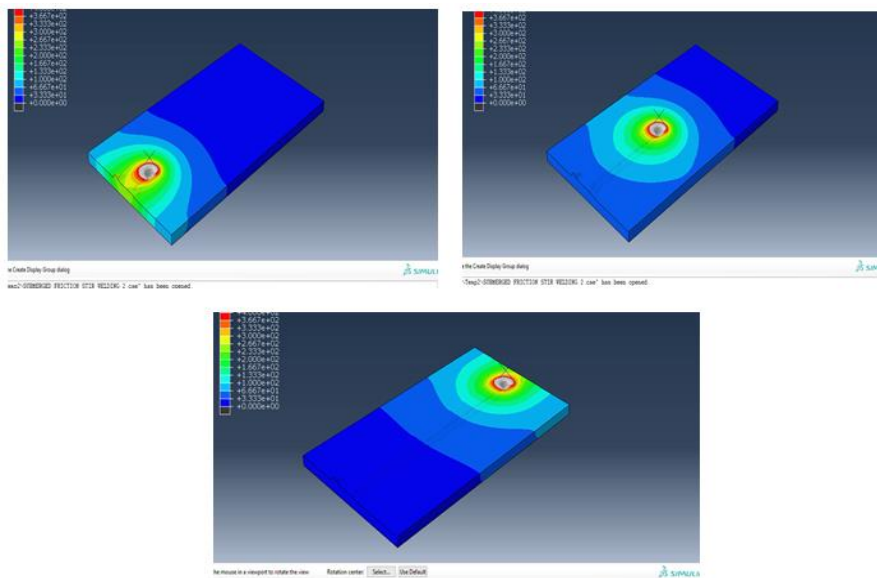


Figure 4. 13 Temperature at various positions (ABAQUS)

At a rotational speed of 1400 rpm and a traverse speed of 15 mm/min, the greatest peak temperature of 368.211°C was reached. Similarly, the lowest temperature of 275.254°C was recorded at 900 rpm and 30 mm/min, respectively. In comparison to the simulation results, minimal temperature difference range was created on the experimental works based on the result.

4.5.1. Comparison of Experimental and Numerical result

4.5.1.1. Comparison of temperature distribution

In the experiment, a thermometer was used to measure the temperature distribution on the weld surface. The temperature measurement was taken across the sheet's breadth and the temperature was measured within 5 second differences at each point. It was measured at the interface between the tool shoulder and the work piece. Five different points were taken each with 15mm distance. The figure at the right side is advancing side and the left is retreating side.

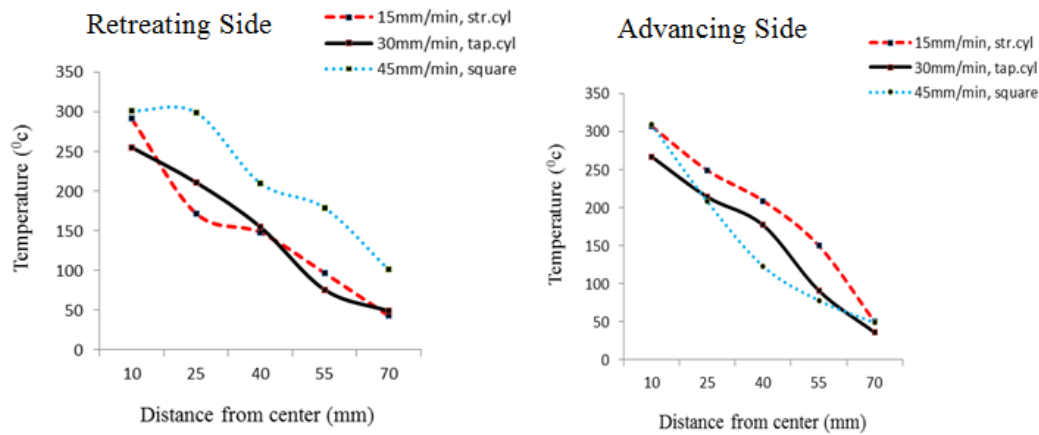


Figure 4. 14 Temperature along the surface at rotational speed of 900 RPM

The peak temperature in Advancing side found by the numerical model was 2.99% larger than the temperature measured experimentally at 900 rpm with 30 mm/min which is the greatest % variation in AS of simulation & experimental temp under 900 RPM experiments. The peak temperatures between the advancing and retreating sides were similar in simulated temperature.

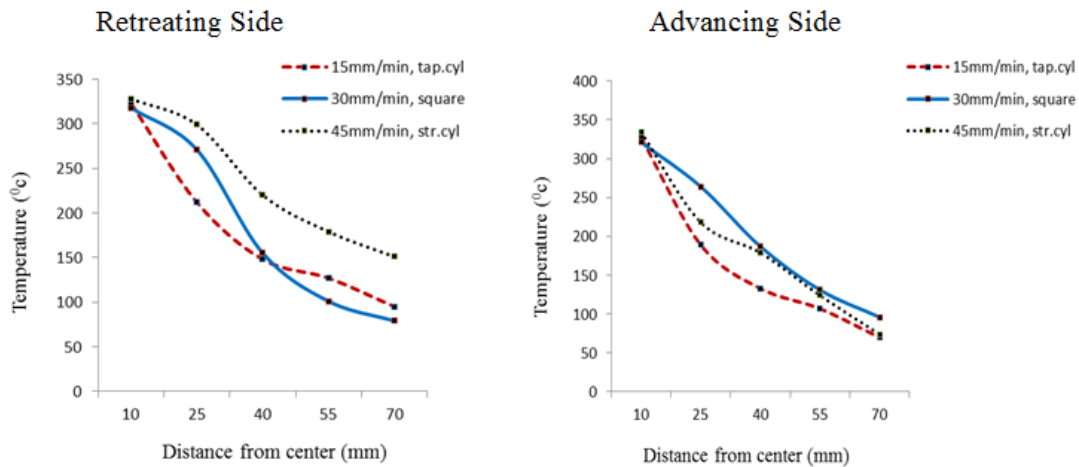


Figure 4. 15 Temperature along the surface at rotational speed of 1200 RPM

The least variation in temperature observed 0.72 % at 1200 Rpm and 15mm/min combination. And this is the least % variation of all samples. The greatest % variation of three 1200 RPM samples was observed under 30mm/min, square pin combination.

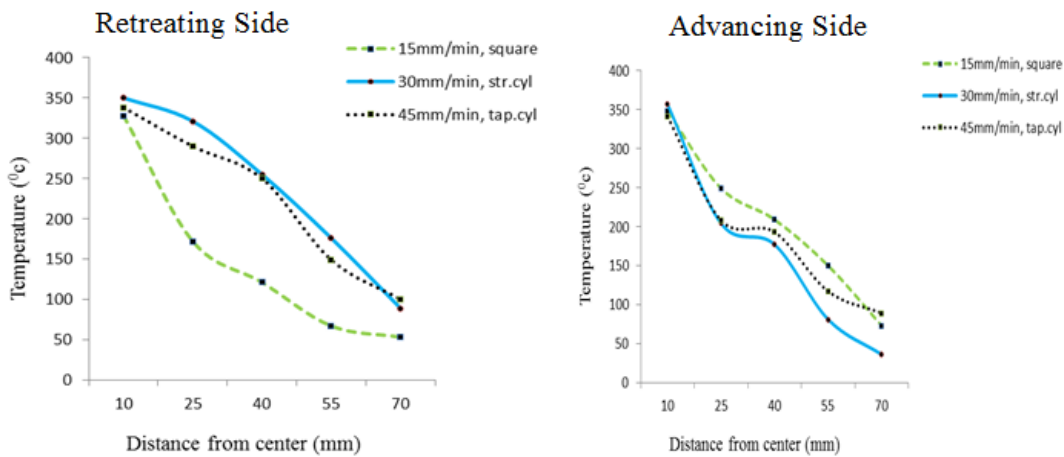


Figure 4. 16 Temperature along the surface at rotational speed of 1400 RPM

Compared to experimental results under 1400 RPM, the greater difference in temperature was observed by 15mm/min and square pin combination resulting 5.48% variation and it was followed by 5.12% variation for 45mm/min, taper cylindrical pin combination.

Finally, for all three rotational speeds, the peak temperature measured by the finite element model matched the observed readings. In addition, the temperature differential between the advancing and retreating sides was very close to the experimental data.

Table 4. 4 Experimental and simulated temperature comparison

No.	Simulation Temperature [°C]		Experiment Temperature [°C]		% Variation in AS of simulation & experimental temp
	Advancing side	Retreating side	Advancing side	Retreating side	
1	311.154	311.154	307	291	1.34
2	275.254	275.254	267	255	2.99
3	314.8	314.8	309	301	1.84
4	329.31	329.31	327	323	0.72
5	330.7	330.7	321	318	2.9
6	341.075	341.075	334	328	2.07
7	368.211	368.211	348	337	5.48
8	350.9	350.9	357	343	1.71
9	359.417	359.417	341	336	5.12

To summarize, the temperature result from the experiment is closer to the modeling results. This indicates that there was a minor temperature measurement error. As a result, the experimental temperature values were securely measured while welding.

4.5.1.2. Comparison of tensile test result

The same property and dimension with the experimental parent material were used to compare the stress-strain result of the Numerical value. Figure 4.15 shows finite element of parent material.

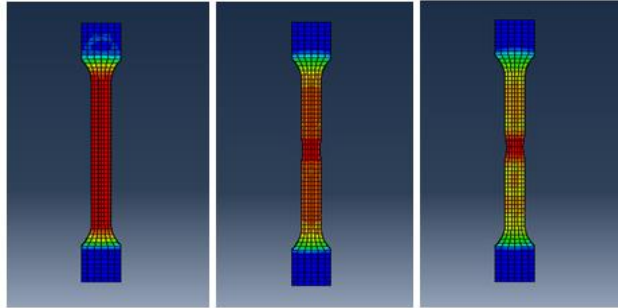


Figure 4. 17 FE test specimen after applying load

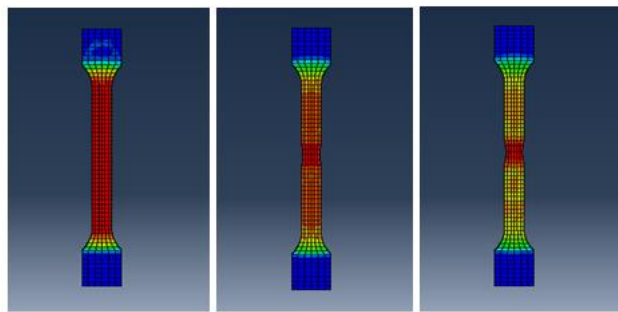


Figure 4. 18 FE test specimen at breaking stage

The numerical result for stress-strain curve is very close to the experimental. It shows that tensile result became 163MPa and 171MPa for experimental and numerical results respectively.

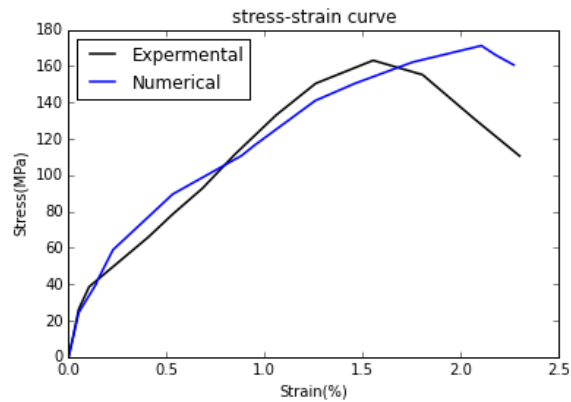


Figure 4. 19 stress-strain curve for experimental and numerical result for AA6063

4.6. Taguchi-based analysis

The Taguchi technique offers three possibilities for calculating the signal-to-noise (S/N) ratio: greater is better, nominal is best, and smaller is best. The selection of a suitable S/N ratio, on the other hand, necessitates some practical experience, competence, and understanding of the process. The goal of this research is to determine which materials have higher tensile strength and hence perform better when welding. The following equation was used for the calculation.

$$\frac{S}{N} (\eta) = -10 \times \log_{10} \frac{1}{n} \sum_{i=1}^n \frac{1}{y^2} \quad 4.1$$

The S/N ratio for the tensile strength is presented in table below.

Table 4. 5 Tensile result and S/N ratio

Exp.No	UTS (MPa)	S/N _{UTM}
1.	113	41.0616
2.	96	39.6454
3.	85	38.5884
4.	71	37.0252
5.	116	41.2892
6.	57	35.1175
7.	102	40.1720
8.	151	43.5795
9.	129	42.2118

4.7. Analysis of S/N Ratios for UTS

In current study the greater S/N Ratio was selected. As a result, the higher parameter's delta value was the better. The best circumstances for this method were found by sorting the delta in order of how much it affected the operation. The larger the delta value, the greater the effect of the parameter.

Below Table presents the calculations of S/N Ratios for tensile strength results using the Minitab design of experiments.

Table 4. 6 Response Table for Signal to Noise Ratios for Larger is better

Level	Rpm	Traverse Speed	Tool Shape
1	39.77	39.42	39.92
2	37.81	41.50	39.63
3	41.99	38.64	40.02
Delta	4.18	2.87	0.39
Rank	1	2	3

Delta = (maximum S/N ratio – minimum S/N ratio).

According to the tensile strength chart and the Response table for Signal to Noise Ratios, RPM had the biggest influence (Delta = 4.18, Rank = 1). Traverse speed was the second most influential parameter affecting the S/N ratio with Delta = 2.87.

The highest plots of each parameter were picked, with the rationale that the larger the ratio set, the better. The delta value shows the same optimum conditions; hence the optimum conditions derived by this method are as follows: Square tool form, 1400 RPM, 30 TS (mm/min).

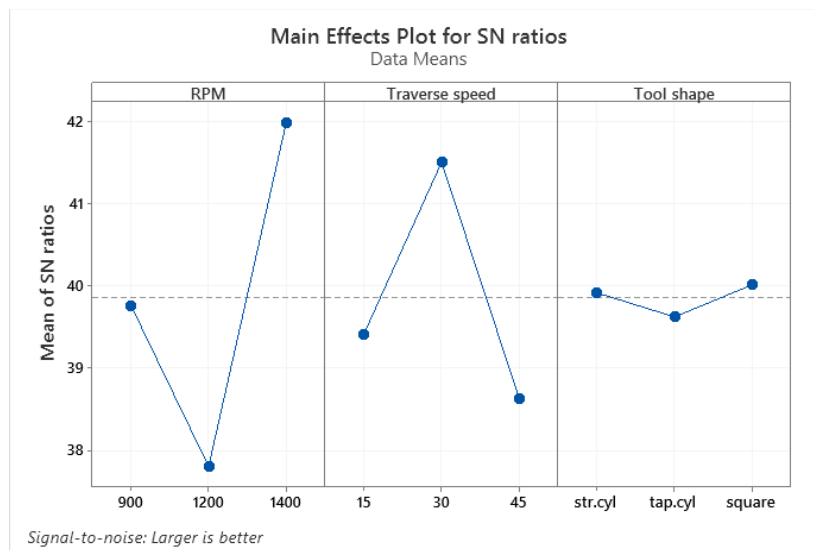


Figure 4. 20 Main effects plot for S/N ratio

4.8. ANOVA result

ANOVA is a statistically-based, objective decision-making approach for identifying differences in the average performance of groups of things. ANOVA aids in formally analysing the importance of the key components and their interactions by comparing the mean square against

an estimate of the experimental errors at particular confidence levels. To begin, subtract the overall mean S/N ratio \bar{m} from the whole sum of squared variances SST:

$$SS_T = \sum_{i=1}^n (n_i - \bar{m})^2 \quad 4.2$$

Where “n” is the number of experiments in the orthogonal array and η_i is the mean S/N ratio for the i^{th} experiment.

Table 4. 7 ANOVA for Tensile Strength

Source	DF	Seq SS	Adj SS	Adj MS	F	P	Contribution
Rpm	2	25.2091	25.2091	13.1045	1.69	0.372	44.90%
Traverse Speed	2	10.1677	10.1677	6.5839	0.85	0.541	18.11%
Tool Shape	2	16.2461	16.2461	0.1230	0.02	0.984	28.94%
Error	2	4.5170	4.5170	7.7585			8.05%
Total	8	56.1399					100.00%

The "F" test can be used to examine whether design parameters have a significant impact on a quality characteristic statistically. The F-ratio is used to assess the significance of a factor in a study. It's the mean square error divided by the residual error.

The P-value reflects the level of significance. The relevance rate of the process parameters on Tensile strength is defined as percent (%). The percent statistics show that RPM, Traverse speed, and Tool shape all have a significant impact on Ultimate tensile strength. RPM, Traverse speed, and Tool shape all had 44.90 percent, 18.11 percent, and 28.94 percent effects on tensile strength, respectively.

4.9. Verification/Confirmation Test

The final step in validating the Taguchi design technique results is the experimental confirmation test. The verification test was used to ensure that the expected value was correct. The forecasted result illustrates 43.8000.

Prediction

<u>S/N Ratio</u>	<u>Mean</u>
43.8000	144.889

Figure 4. 21 prediction by Minitab

CHAPTER FIVE

CONCLUSION AND RECOMMENDATION

5.1. Conclusion

6063 AA material was considered in the current investigation to assess the impact of process parameters on the tensile strength with butt joint configuration of SFSW. After completing the experimental task, FE approach were conducted to evaluate the impact of process factors. A variety of welding parameters were investigated to achieve excellent joints, including rotational speed and tool pin profile. Taguchi method optimization technique was used to determine the

best conditions for SFSW parameters in order to investigate the impact of many factors on mechanical strength, such as UTS. An experimental design was created using the mixed L9 orthogonal array and the data collected from the experiments was analysed. Nine experiments were conducted and rotational speed, tool shape, and traverse speed becomes significant with a joint efficiency of about 91.8%. The following are the conclusions based on the results of finite element and experimental investigation.

1. The maximum tensile strength was found at the rotational speed of 1400 rpm, 30mm/min traverse speed and straight cylindrical tool shape combination due to adequate heat generation and proper cooling effect resulting 151MPa. And the minimum UTS were recorded 57MPa using 1200 RPM.
2. According to the study the RPM was the most influential factor for joint strength followed by traverse speed and tool pin profile. The maximum temperature from the simulation was observed at the square tool profile at 15 mm/min welding speed and 1400 rpm rotational speed.
3. Due to high heat input and low feed rate, the better microscopic images were observed at 1200 RPM with 30mm/min and 1400 RPM with 30mm/min.

The study's results can be summed up as follows:

- It has been successful to produce welds with good tensile and microstructural qualities that are close to the source material using submerged friction stir welding. The characteristics like mechanical and microstructural properties could be greatly improved by controlling the process parameters.
- Due to the reduction in heat input caused by immersion in water, there were less voids in the material, which improved the tensile strength. The frictional heat input increased as the RPM increased. It was discovered that the comparatively high rotational speed produced good weld joint characteristics. The creation of void and flash flaws caused by inappropriate stirring at very low rotational speeds. Traverse speed, in addition to RPM, is a key factor in regulating the heat input. It has been demonstrated that the peak temperature was somewhat raised when traverse speed increases.
- Lagrangian finite element formulation was found to be challenging to simulate because the high plastic deformation created an excessive amount of mesh distortion. A extremely thin

mesh and remesh techniques were used in an effort to solve this problem. By adjusting the boundary condition temperature in the Eulerian-Lagrangian formulation, the FE simulation of the SFSW process was successfully completed. Using the findings of the experiments, the peak temperatures in the advancing and retreating sides as well as the thermal profiles were successfully predicted and validated.

5.2. Recommendations and Future Work

It was difficult to find a universal tensile machine with the gripper size as needed. It would be preferable if the university considered giving the machines in order to expand its manufacturing and mechanical testing research.

- ✓ The scope of this study was limited to aluminium alloys of identical composition. It can, however be used to a variety of different materials and polymers.
- ✓ The hardness test was not explored in this study. It can be performed and compared to parent material. And also the research was conducted in butt welding, but it can also be used for lap welding and T-welding.
- ✓ Additional process parameters such as axial force, dwell time, and plunger depth might be included and their influence on joint quality investigated as well.
- ✓ Different water temperatures can be used to do additional research on submerged FSW. Other coolants may also be employed to further regulate grain development during the operation.

REFERENCE

- Abaqus 6.11. 2011. *Analysis User's Manual Volume I: Introduction, Spatial Modeling, Execution & Output*.
- American Welding Society, U S A. 2006. *Materials & Design Specifications for Friction Stir Welding of Aluminum Alloys for Aerospace Applications*.
- Besharati-Givi, Mohammad Kazem, and Parviz Asadi. 2014. *Advances in Friction-Stir Welding and Processing*. Elsevier.
- Bijanrostami, Khosro, and Reza Vatankhah Barenji. 2019. "Underwater Dissimilar Friction Stir Welding of Aluminum Alloys: Elucidating the Grain Size and Hardness of the Joints."

-
- Proceedings of the Institution of Mechanical Engineers, Part L: Journal of Materials: Design and Applications* 233(4): 763–75.
- Celik, Sare, and Recep Cakir. 2016. “Effect of Friction Stir Welding Parameters on the Mechanical and Microstructure Properties of the Al-Cu Butt Joint.” *Metals* 6(6): 133.
- Chandrashekar, A, B S Ajay Kumar, and H N Reddappa. “Friction Stir Welding : Tool Material and Geometry.” *AKGEC INTERNATIONAL JOURNAL OF TECHNOLOGY* 6(1): 16–20.
- Chen, Kai, Xun Liu, and Jun Ni. 2017. “Effects of Process Parameters on Friction Stir Spot Welding of Aluminum Alloy to Advanced High-Strength Steel.” *Journal of Manufacturing Science and Engineering* 139(8).
- Dalle Donne, C et al. 2001. “Investigations on Residual Stresses in Friction Stir Welds.”
- Davis, Joseph R. 2001. *Alloying: Understanding the Basics*. ASM international.
- Dhas, J Edwin Raja, and S Jenkins Hexley Dhas. 2012. “A Review on Optimization of Welding Process.” *Procedia Engineering* 38: 544–54.
- Dubourg, L, and P Dacheux. 2006. “Design and Properties of FSW Tools: A Literature Review.” In *Proceedings of 6th International Symposium on Friction Stir Welding, Saint-Sauveur, Quebec, Canada*,.
- Elangovan, K, and V Balasubramanian. 2008. “Materials & Design Influences of Tool Pin Profile and Tool Shoulder Diameter on the Formation of Friction Stir Processing Zone in AA6061 Aluminium Alloy.” *science Direct* 29: 362–73.
- Eldin, Emad, and Mohammed Kishta. 2014. “INVESTIGATION OF SUBMERGED FRICTION STIR WELDING OF MARINE-GRADE ALUMINUM ALLOY.” (January).
- Garg, Tulika et al. 2014. “Underwater Friction Stir Welding: An Overview.” *International Review of Applied Engineering Research* 4(2): 165–70.
- Ghetiya, N D, and K M Patel. 2015. “Prediction of Tensile Strength and Microstructure Characterization of Immersed Friction Stir Welding of Aluminium Alloy AA2014-T4.”
- Ghetiya, Nilesh D, and Kaushik M Patel. 2017. “Welding Speed Effect on Joint Properties in Air and Immersed Friction Stir Welding of AA2014.” *Proceedings of the Institution of Mechanical Engineers, Part B: Journal of Engineering Manufacture* 231(5): 897–909.
- Gibson, Brian T et al. 2014. “Friction Stir Welding: Process, Automation, and Control.” *Journal of Manufacturing Processes* 16(1): 56–73.
- Gomathisankar, M, M Gangatharan, and P Pitchipoo. 2018. “ScienceDirect A Novel

-
- Optimization of Friction Stir Welding Process Parameters on Aluminum Alloy 6061-T6.” *Materials Today: Proceedings* 5(6): 14397–404. <https://doi.org/10.1016/j.matpr.2018.03.025>.
- Hilgert, J, H N B Schmidt, J F Dos Santos, and N Huber. 2011. “Thermal Models for Bobbin Tool Friction Stir Welding.” *Journal of Materials Processing Technology* 211(2): 197–204.
- Hofmann, Douglas C., and Kenneth S. Vecchio. 2005. “Submerged Friction Stir Processing (SFSP): An Improved Method for Creating Ultra-Fine-Grained Bulk Materials.” *Materials Science and Engineering A* 402(1–2): 234–41.
- Hussain, Mohd Azmal, Noor Zaman Khan, Arshad Noor Siddiquee, and Zahid Akhtar Khan. 2018. “Effect of Different Tool Pin Profiles on the Joint Quality of Friction Stir Welded AA 6063.” *Materials Today: Proceedings* 5(2): 4175–82.
- Jain, Rahul, Surjya K Pal, and Shiv B Singh. 2017. *Computational Methods and Production Engineering Numerical Modeling Methodologies for Friction Stir Welding Process*. Elsevier Ltd. <http://dx.doi.org/10.1016/B978-0-85709-481-0.00005-7>.
- Joshi, Saumil K, and Jaivesh D Gandhi. 2015. “Influence of Tool Shoulder Geometry on Friction Stir Welding: A Literature Review.” *2nd International Conference on Multidisciplinary Research & Practice III(I)*: 261–64.
- Kaviyarasan, K et al. 2020. “Comparison of Mechanical Properties of Al6063 Alloy with Ceramic Particles.” *Materials Today: Proceedings* 22: 3067–74.
- Khalilabad, Mahdi Masoumi et al. 2016. “The Influence of Tool Geometry on Mechanical Properties of Friction Stir Welded AA-2024 and AA-2198 Joints.” In *34th CONFERENCE AND EXHIBITION ICSOBA*.
- Khan, Noor Zaman, Zahid A Khan, and Arshad Noor Siddiquee. 2015. “Effect of Shoulder Diameter to Pin Diameter (D/d) Ratio on Tensile Strength of Friction Stir Welded 6063 Aluminium Alloy.” *Materials Today: Proceedings* 2(4–5): 1450–57.
- Khan, Noor Zaman, Arshad Noor Siddiquee, and Zahid A Khan. 2017. *Friction Stir Welding: Dissimilar Aluminum Alloys*. CRC Press.
- Khan, Noor Zaman, Arshad Noor Siddiquee, Zahid A Khan, and Suha K Shihab. 2015. “Investigations on Tunneling and Kissing Bond Defects in FSW Joints for Dissimilar Aluminum Alloys.” *Journal of alloys and Compounds* 648: 360–67.
- Khandkar, Mir Zahedul H, Jamil A Khan, Anthony P Reynolds, and Michael A Sutton. 2006.

-
- “Predicting Residual Thermal Stresses in Friction Stir Welded Metals.” 174(May 2005): 195–203.
- Kishta, Emad Eldin, and Basil Darras. 2016. “Experimental Investigation of Underwater Friction-Stir Welding of 5083 Marine-Grade Aluminum Alloy.” *Proceedings of the Institution of Mechanical Engineers, Part B: Journal of Engineering Manufacture* 230(3): 458–65.
- Konkol, Paul J, and Mark F Mruczek. 2007. “Comparison of Friction Stir Weldments and Submerged Arc Weldments in HSLA-65 Steel.” *WELDING JOURNAL-NEW YORK-* 86(7): 187.
- Li, Gaohui et al. 2019. “Influence of Dwell Time on Microstructure Evolution and Mechanical Properties of Dissimilar Friction Stir Spot Welded Aluminum–Copper Metals.” *Journal of Materials Research and Technology* 8(3): 2613–24.
- Liu, H J, H J Zhang, and Lei Yu. 2011. “Effect of Welding Speed on Microstructures and Mechanical Properties of Underwater Friction Stir Welded 2219 Aluminum Alloy.” *Materials & Design* 32(3): 1548–53.
- Liu, Hui-Jie, Hui-jie Zhang, Yong-xian Huang, and Y U Lei. 2010. “Mechanical Properties of Underwater Friction Stir Welded 2219 Aluminum Alloy.” *Transactions of Nonferrous Metals Society of China* 20(8): 1387–91.
- Meilinger, Ákos, and Imre Török. 2013. “The Importance of Friction Stir Welding Tool.” *Production Processes and Systems* 6(1): 25–34.
- Mishra, Rajiv S, and Harpreet Sidhar. 2016. *Friction Stir Welding of 2xxx Aluminum Alloys Including Al-Li Alloys*. Butterworth-Heinemann.
- Mishra, Rajiv Sharan, Partha Sarathi De, and Nilesh Kumar. 2014. “Friction Stir Processing.” In *Friction Stir Welding and Processing*, Springer, 259–96.
- Mofid, Mohammad Ammar, Amir Abdollah-Zadeh, Farshid Malek Ghaini, and Cemil Hakan Gür. 2012. “Submerged Friction-Stir Welding (SFSW) Underwater and under Liquid Nitrogen: An Improved Method to Join Al Alloys to Mg Alloys.” *Metallurgical and Materials Transactions A: Physical Metallurgy and Materials Science* 43(13): 5106–14.
- Mohamadreza, Nourani, Milani Abbas S, and Yannacopoulos Spiro. 2011. “Taguchi Optimization of Process Parameters in Friction Stir Welding of 6061 Aluminum Alloy: A Review and Case Study.” *Engineering* 2011.

-
- Papahn, Hossein, Pouya Bahemmat, Mohammad Haghpanahi, and Christof Sommitsch. 2015. "Study on Governing Parameters of Thermal History during Underwater Friction Stir Welding." *International Journal of Advanced Manufacturing Technology* 78(5–8): 1101–11.
- Peel, M, A Steuwer, M Preuss, and P J Withers. 2003. "Microstructure , Mechanical Properties and Residual Stresses as a Function of Welding Speed in Aluminium AA5083 Friction Stir Welds." 51: 4791–4801.
- Rogalski, Grzegorz, Dariusz Fydrych, and Jerzy Łabanowski. 2017. "Underwater Wet Repair Welding of API 5L X65M Pipeline Steel." *Polish Maritime Research*.
- Roy, Ranjit K. 2010. *A Primer on the Taguchi Method*. Society of Manufacturing Engineers.
- Rui-dong, Fu et al. 2011. "Improvement of Weld Temperature Distribution and Mechanical Properties of 7050 Aluminum Alloy Butt Joints by Submerged Friction Stir Welding." *Materials and Design* 32(10): 4825–31. <http://dx.doi.org/10.1016/j.matdes.2011.06.021>.
- Sabari, S Sree, S Malarvizhi, and V Balasubramanian. 2016a. "INFLUENCES OF TOOL TRAVERSE SPEED ON TENSILE PROPERTIES OF AIR COOLED AND WATER COOLED FRICTION STIR WELDED AA2519-T87 ALUMINIUM ALLOY JOINTS." *Journal of Materials Processing Tech*. <http://dx.doi.org/10.1016/j.jmatprotec.2016.06.015>.
- . 2016b. "The Effect of Pin Profiles on the Microstructure and Mechanical Properties of Underwater Friction Stir Welded AA2519-T87 Aluminium Alloy." *International Journal of Mechanical and Materials Engineering* 11(1): 1–14.
- Said, MTSM et al. 2015. "The Effect of Pin Size on Friction Stir Welded AA5083 Plate Lap Joint." In *International Conference on Production, Automobiles and Mechanical Engineering*, , 87–92.
- Saravanan, V, S Rajakumar, Nilotpal Banerjee, and R Amuthakkannan. 2016. "Effect of Shoulder Diameter to Pin Diameter Ratio on Microstructure and Mechanical Properties of Dissimilar Friction Stir Welded AA2024-T6 and AA7075-T6 Aluminum Alloy Joints." *The International Journal of Advanced Manufacturing Technology*. <http://dx.doi.org/10.1007/s00170-016-8695-0>.
- Schmidt, H, Jesper Hattel, and John Wert. 2003. "An Analytical Model for the Heat Generation in Friction Stir Welding." *Modelling and simulation in materials science and engineering* 12(1): 143.

-
- Schmidt, Hattel, and Jesper Hattel. 2004. "A Local Model for the Thermomechanical Conditions in Friction Stir Welding." *Modelling and simulation in materials science and engineering* 13(1): 77.
- Sevvel, P, and V Jaiganesh. 2017. "ScienceDirect Effects of Axial Force on the Mechanical Properties of AZ80A Mg Alloy during Friction Stir Welding." *Materials Today: Proceedings* 4(2): 1312–20. <http://dx.doi.org/10.1016/j.matpr.2017.01.152>.
- Shercliff, Hugh R, Paul A Colegrove, R S Mishra, and M W Mahoney. 2007. "Process Modeling." *Friction stir welding and processing*: 187–217.
- Shinde, Ram D, and Mahendra G Rathi. 2016. "OPTIMIZATION OF FSW PROCESS PARAMETER TO ACHIEVE MAXIMUM TENSILE STRENGTH OF ALUMINUM ALLOY AA6061." : 936–43.
- Singh, Kulwant, Gurbhinder Singh, and Harmeet Singh. 2018. "Review on Friction Stir Welding of Magnesium Alloys." 6: 399–416.
- Soundararajan, Vijay, Srdja Zekovic, and Radovan Kovacevic. 2005. "Thermo-Mechanical Model with Adaptive Boundary Conditions for Friction Stir Welding of Al 6061." *International journal of machine tools and manufacture* 45(14): 1577–87.
- Sun, Seung-ju et al. 2017. "Influence of Friction Stir Welding on Mechanical Properties of Butt Joints of AZ61 Magnesium Alloy." 2017.
- Threadgill, P L. 1997. "Friction Stir Welds in Aluminium Alloys-Preliminary Microstructural Assessment." *TWI Bulletin*: 30–33.
- Tolcha, M A, and L E Melaku. 2020. "Experimental and Parametric Analyzing of Friction Stir Welding for AA-6061 Aluminum Alloys." *ADRRI Journal of Engineering and ...* (February). <https://journals.adrri.org/index.php/adrrijet/article/view/508>.
- Upadhyay, P, and Anthony P Reynolds. 2010. "Effects of Thermal Boundary Conditions in Friction Stir Welded AA7050-T7 Sheets." *Materials Science and Engineering: A* 527(6): 1537–43.
- Venkateswarlu, D, N R Mandal, M M Mahapatra, and S P Harsh. 2013. "Tool Design Effects for FSW of AA7039." *Welding Journal* 92(2): 41–47.
- Verduzco Juárez, J C, I G M Dominguez Almaraz, R García Hernández, and J J Villalón López. 2016. "Effect of Modified Pin Profile and Process Parameters on the Friction Stir Welding of Aluminum Alloy 6061-T6." *Advances in Materials Science and Engineering* 2016.

-
- Verma, S, M Gupta, and J P Misra. 2016. "Friction Stir Welding of Aerospace Materials: A State of Art Review." *Chapter 13*: 135–50.
- WAHID, Mohd Atif, Zahid A. KHAN, and Arshad Noor SIDDIQUEE. 2018. "Review on Underwater Friction Stir Welding: A Variant of Friction Stir Welding with Great Potential of Improving Joint Properties." *Transactions of Nonferrous Metals Society of China (English Edition)* 28(2): 193–219. [http://dx.doi.org/10.1016/S1003-6326\(18\)64653-9](http://dx.doi.org/10.1016/S1003-6326(18)64653-9).
- Wang, Qingzhao, Zhixia Zhao, Yong Zhao, et al. 2015a. "The Adjustment Strategy of Welding Parameters for Spray Formed 7055 Aluminum Alloy Underwater Friction Stir Welding Joint." *JMADE*. <http://dx.doi.org/10.1016/j.matdes.2015.09.038>.
- . 2015b. "The Adjustment Strategy of Welding Parameters for Spray Formed 7055 Aluminum Alloy Underwater Friction Stir Welding Joint." *Materials & Design* 88: 1366–76.
- Wang, Qingzhao et al. 2016. "The Strengthening Mechanism of Spray Forming Al-Zn-Mg-Cu Alloy by Underwater Friction Stir Welding." *Materials & Design* 102: 91–99.
- Wang, Qingzhao, Yong Zhao, Keng Yan, and Sheng Lu. 2015. "Corrosion Behavior of Spray Formed 7055 Aluminum Alloy Joint Welded by Underwater Friction Stir Welding." *Materials & Design* 68: 97–103.
- Williams, S W, and A Steuwer. 2010a. "Residual Stresses in Friction Stir Welding." In *Friction Stir Welding: From Basics to Applications*, Woodhead Publishing Limited, 215–44. <http://dx.doi.org/10.1533/9781845697716.2.215>.
- . 2010b. "Residual Stresses in Friction Stir Welding." In *Friction Stir Welding*, Elsevier, 215–44.
- XU WF, LIUJH, D L CHEN, G H LUAN, and J S YAO. 2012. "Improvements of Strength and Ductility in Aluminum Alloy Joints via Rapid Cooling during Friction Stir Welding [J]." *Materials Science and Engineering A* 548: 89–98.
- Zhang, H J, H J Liu, and L Yu. 2011. "Microstructure and Mechanical Properties as a Function of Rotation Speed in Underwater Friction Stir Welded Aluminum Alloy Joints." 32: 4402–7.
- . 2012. "Effect of Water Cooling on the Performances of Friction Stir Welding Heat-Affected Zone." 21(7): 1182–87.
- Zhang, Huijie, and Huijie Liu. 2012. "Characteristics and Formation Mechanisms of Welding

-
- Defects in Underwater Friction Stir Welded Aluminum Alloy.” *Metallography, Microstructure, and Analysis* 1(6): 269–81.
- . 2013. “Mathematical Model and Optimization for Underwater Friction Stir Welding of a Heat-Treatable Aluminum Alloy.” *JOURNAL OF MATERIALS&DESIGN* 45: 206–11. <http://dx.doi.org/10.1016/j.matdes.2012.09.022>.
- Zhang, Zhao, and H W Zhang. 2009. “Numerical Studies on Controlling of Process Parameters in Friction Stir Welding.” *Journal of materials processing technology* 209(1): 241–70.
- Zhao, Yong, Lilong Zhou, et al. 2014. “Defects and Tensile Properties of 6013 Aluminum Alloy T-Joints by Friction Stir Welding.” *Materials & Design* 57: 146–55.
- Zhao, Yong et al. 2016. “Influence of Cooling Conditions on Joint Properties and Microstructures of Aluminum and Magnesium Dissimilar Alloys by Friction Stir Welding.” : 673–79.
- Zhao, Yong, Zhengping Lu, Keng Yan, and Linzhao Huang. 2015. “Microstructural Characterizations and Mechanical Properties in Underwater Friction Stir Welding of Aluminum and Magnesium Dissimilar Alloys.” *Materials & Design (1980-2015)* 65: 675–81.
- Zhao, Yong, Qingzhao Wang, Huabin Chen, and Keng Yan. 2014. “Microstructure and Mechanical Properties of Spray Formed 7055 Aluminum Alloy by Underwater Friction Stir Welding.” *JOURNAL OF MATERIALS&DESIGN* 56: 725–30. <http://dx.doi.org/10.1016/j.matdes.2013.11.071>.

APPENDIX

Appendix 1: AA 6063 composition test result



በ ኢትዮ-ኢንጅነሪንግ ግሩፕ
የ አዲስ ማሽንና መለዋወጫ ማምረቻ ኢንዱስትሪ
Ethio-engineering Group
Addis Machine and Spare Part Manufacturing Industry

ጽ/ቤት አድራሻ

ቀን

Date: 04/12/2013

Requested by: ABENEZER ABTAYE

Sample type: ALUMINIUM

Purpose: IDENTIFICATION

S/N	Sample Name	Chemical Composition												
		Si	Fe	Cu	Mn	Mg	Zn	Ni	Cr	Pb	Ti	V	Al	CSN
1	FRAME	0.43	0.57	0.014	0.013	0.87	0.0080	0.058	0.061	0.060	0.075	0.026	96.9	Aluminum

Prepared by: Y. halem

Checked by: Y. halem

Approved by: Kebede

Sign: [Signature]

Sign: [Signature]

Sign: [Signature]

Date: 04/12/13

Date: 04/12/13

Date: 04/12/13



ስልክ ጽ/ቤት +251 115 508 685 /የኮምፒውተር አገልግሎት/
Tell +251 115 508 690/የኮምፒውተር አገልግሎት/
+251 115 520 565/የኮምፒውተር አገልግሎት/
addis@industrialmail.com

ፖ.ሣ.ጽ/ቤት 583
P.O.Box

ፋክስ +251 115 545 405
Fax
ኢ-ሜይል

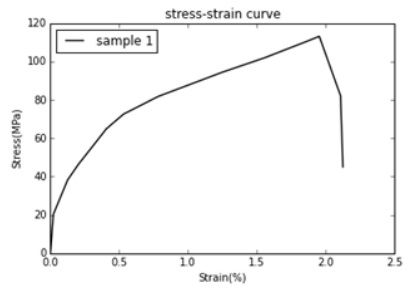
industrialmail.com

Appendix 2: Tensile test output for each samples

Code: WP 310
 G.U.N.T. Gerätebau GmbH
 Hanskampring 15 -17,
 22885 Barsbüttel
 Germany, Tel ++4940 / 67 08 54 -0
 Date: 26.11.2021 Time: 06:52:05

Name: T2
 User Comment:
 Sample: 1

Strain (%)	Stress (Mpa)
0	0
0.0216	12.366
0.2006	34.3019
0.3047	54.5729
0.4062	58.875
0.5312	63.5417
0.7828	67.75
1.2475	92.3542
1.5578	99.9583
1.8594	110.3906
1.9531	113.0885
2.1078	67.0573

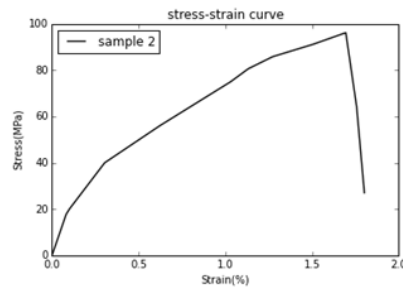


Tool rotation 900 RPM, traverse speed 15mm/min and straight cylindrical pin combination resulting tensile strength of 113 MPa.

Code: WP 310
 G.U.N.T. Gerätebau GmbH
 Hanskampring 15 -17,
 22885 Barsbüttel
 Germany, Tel ++4940 / 67 08 54 -0
 Date: 26.11.2021 Time: 06:58:24

Name: T2
 User Comment:
 Sample: 2

Strain (%)	Stress (Mpa)
0	0
0.0816	30.7344
0.4037	37.9583
0.6219	37.9583
1.0312	41.9687
1.1328	48.5677
1.2734	56.7708
1.5047	85.0677
1.6953	96.125
1.7578	64.215
1.8024	27.0018

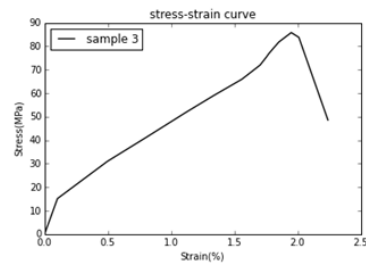


Tool rotation 900 RPM, traverse speed 30mm/min and taper cylindrical pin combination resulting tensile strength of 96 MPa.

Code: WP 310
 G.U.N.T. Gerätebau GmbH
 Hanskampring 15 -17,
 22885 Barsbüttel
 Germany, Tel ++4940 / 67 08 54 -0
 Date: 26.11.2021 Time: 07:14:43

Name: T2
 User Comment:
 Sample: 3

Strain (%)	Stress (Mpa)
0	0
0.1017	10.1302
0.6978	20.0312
0.9918	35.8073
1.1214	38.9704
1.3382	41.8646
1.4117	44.1406
1.5327	49.0349
1.5602	51.9531
1.7038	70.9635
1.7543	76.4323
1.7757	79.0365
1.8518	81.7708
1.9503	85.8073
2.0103	78.776
2.2403	0

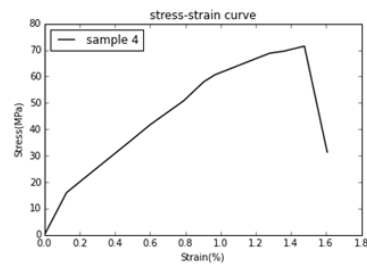


Tool rotation 900 RPM, traverse speed 45mm/min and square pin combination resulting tensile strength of 85 MPa.

Code: WP 310
 G.U.N.T. Gerätebau GmbH
 Hanskampring 15 -17,
 22885 Barsbüttel
 Germany, Tel ++4940 / 67 08 54 -0
 Date: 26.11.2021 Time: 07:21:09

Name: T2
 User Comment:
 Sample: 4

Strain (%)	Stress (Mpa)
0	0
0.4141	7.8125
0.4922	9.7656
0.6016	9.7656
0.7891	13.6719
0.9062	19.0104
0.9687	21.6146
1.2187	39.1927
1.2812	41.7969
1.3594	64.5245
1.4766	71.451
1.6062	31.321
1.6602	0

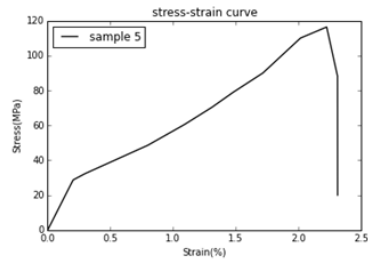


Tool rotation 1200 RPM, traverse speed 15mm/min and taper cylindrical pin combination resulting tensile strength of 71 MPa.

Code: WP 310
G.U.N.T. Gerätebau GmbH
Hanskampring 15 -17,
22885 Barsbüttel
Germany, Tel ++4940 / 67 08 54 -0
Date: 26.11.2021 Time: 07:29:51

Name: T2
User Comment:
Sample: 5

Strain (%)	Stress (Mpa)
0	0
0.1717	10.3302
0.2032	15.7302
0.297	19.3021
0.7982	27.8958
0.8909	30.1094
1.2132	40.4948
1.3085	50.7031
1.3585	45.3073
1.4788	51.9531
1.7162	79.0245
2.0154	99.0178
2.224	116.351
2.3101	88.301
2.3109	0

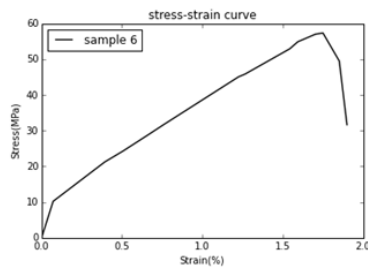


Tool rotation 1200 RPM, traverse speed 30 mm/min and square pin combination resulting tensile strength of 116 MPa.

Code: WP 310
G.U.N.T. Gerätebau GmbH
Hanskampring 15 -17,
22885 Barsbüttel
Germany, Tel ++4940 / 67 08 54 -0
Date: 26.11.2021 Time: 07:36:04

Name: T2
User Comment:
Sample: 6

strain	stress
0	0
0.0716	10.2022
0.3931	27.235
0.5047	25.235
0.6562	32.6354
0.7578	32.6354
1.2253	44.0625
1.2656	40.8281
1.4922	47.1354
1.5937	52.6042
1.5937	52.8698
1.7031	56.9896
1.75	57.3385
1.8516	49.4792
1.8994	39.6667

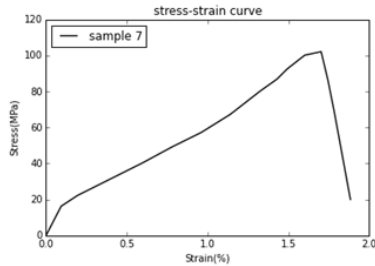


Tool rotation 1200 RPM, traverse speed 45mm/min and straight cylindrical pin combination resulting tensile strength of 57 MPa.

Code: WP 310
 G.U.N.T. Gerätebau GmbH
 Hanskampring 15 -17,
 22885 Barsbüttel
 Germany, Tel ++4940 / 67 08 54 -0
 Date: 26.11.2021 Time: 07:44:05

Name: T2
 User Comment:
 Sample: 7

Strain (%)	Stress(Mpa)
0	0
0.0937	23.2552
0.1953	13.2552
0.5969	36.2969
0.7812	38.2396
0.9609	50.224
1.1406	61.2708
1.3266	64.2708
1.4297	89.8437
1.4922	92.4479
1.6016	100.1354
1.7031	102.0833
1.7452	86.254
1.7844	68.6241
1.8844	20

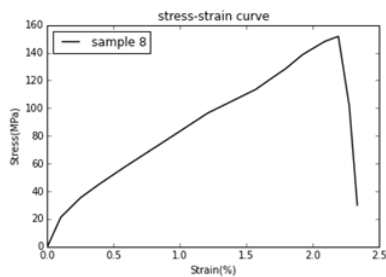


Tool rotation 1400 RPM, traverse speed 15mm/min and square pin combination resulting tensile strength of 102 MPa.

Code: WP 310
 G.U.N.T. Gerätebau GmbH
 Hanskampring 15 -17,
 22885 Barsbüttel
 Germany, Tel ++4940 / 67 08 54 -0
 Date: 26.11.2021 Time: 08:02:31

Name: T2
 User Comment:
 Sample: 8

Strain (%)	Stress (Mpa)
0	0
0.1016	25.3021
0.2501	39.3201
0.3895	34.0014
0.5781	36.2001
0.9062	50.5208
1.1098	65.2541
1.2078	50.3698
1.5703	67.5156
1.6656	76.9531
1.7934	92.3177
1.9219	112.5312
2.0903	139.1406
2.1919	151.7448
2.2344	101.3646
2.3344	0

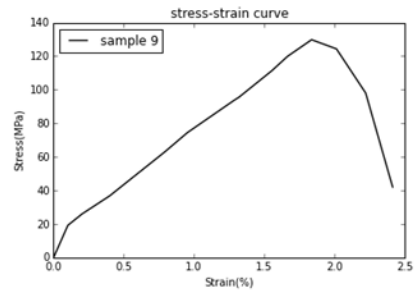


Tool rotation 1400 RPM, traverse speed 30mm/min and straight cylindrical pin combination resulting tensile strength of 151 MPa.

Code: WP 310
G.U.N.T. Gerätebau GmbH
Hanskampring 15 -17,
22885 Barsbüttel
Germany, Tel ++4940 / 67 08 54 -0
Date: 26.11.2021 Time: 08:50:56

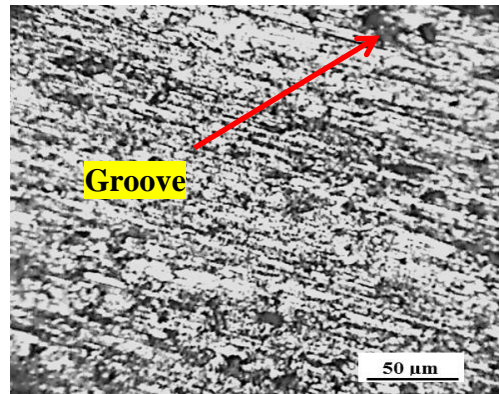
Name: T2
User Comment:
Sample: 9

Data Start	Strain (%)	Stress (Mpa)
	0	0
	0.1016	25.1719
	0.2031	25.9948
	0.3984	29.7083
	0.7891	35.8073
	0.9516	39.4115
	1.2831	50.6198
	1.3203	65.625
	1.5547	98.4583
	1.6641	101.875
	1.8359	129.8177
	2.0125	124.356
	2.2208	98.0014
	2.4125	42

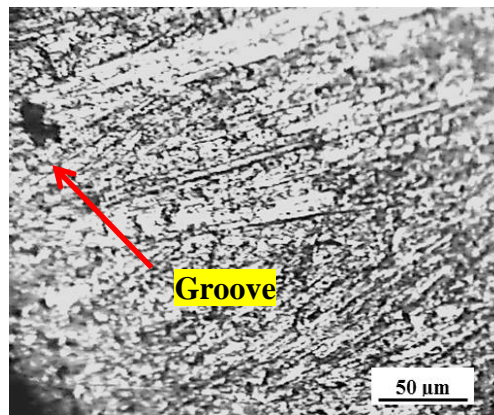


Tool rotation 1400 RPM, traverse speed 45mm/min and taper cylindrical pin combination resulting tensile strength of 129 MPa.

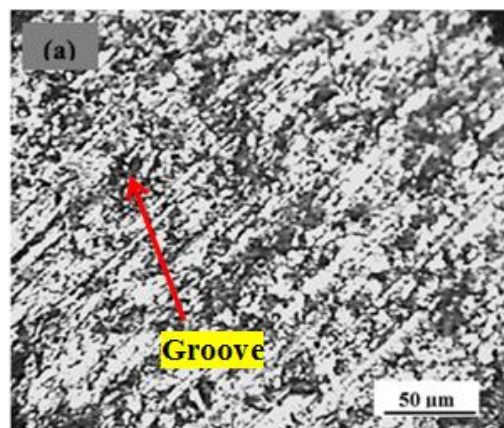
Appendix 3: metallographic image:



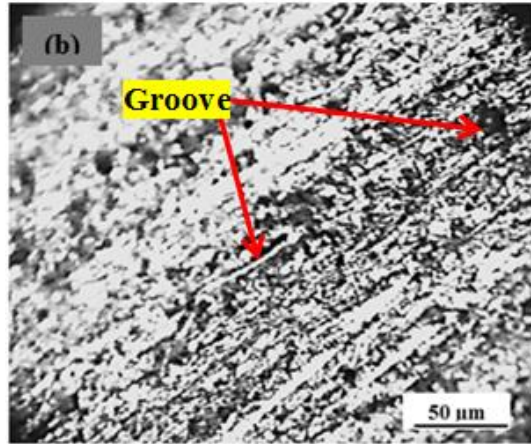
Metallographic image for 900 RPM, traverse speed 15mm/min and straight cylindrical pin combination



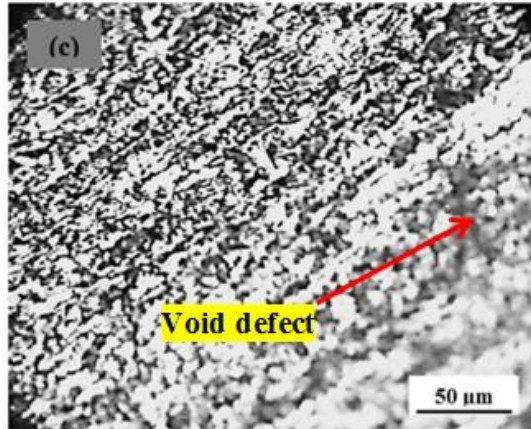
Metallographic image for 900 RPM, traverse speed 30mm/min and taper cylindrical pin combination



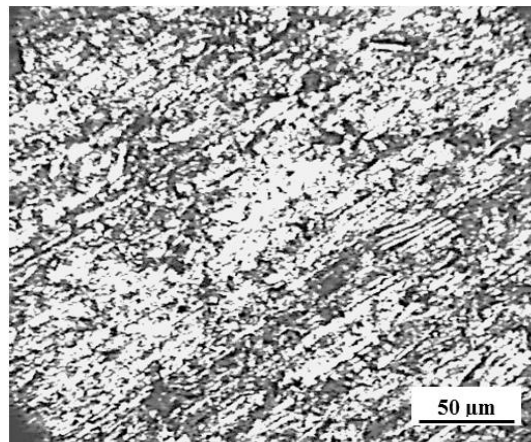
Metallographic image for 900 RPM, traverse speed 45mm/min and square pin combination



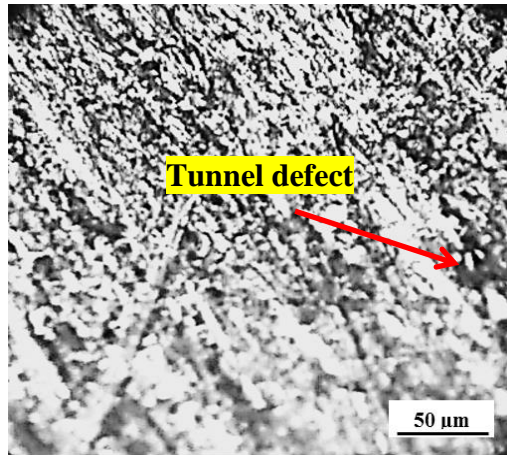
Metallographic image for 1200 RPM, traverse speed 15mm/min and taper cylindrical pin combination



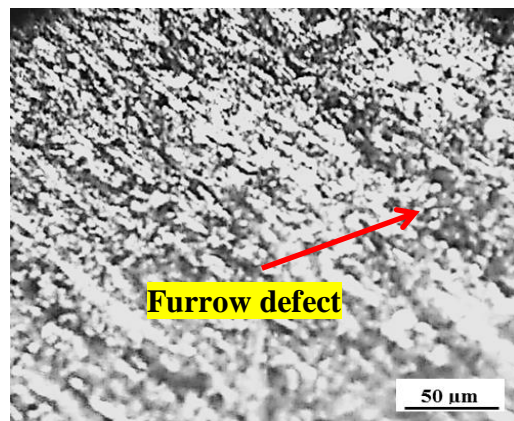
Metallographic image for 1200 RPM, traverse speed 30mm/min and square pin combination



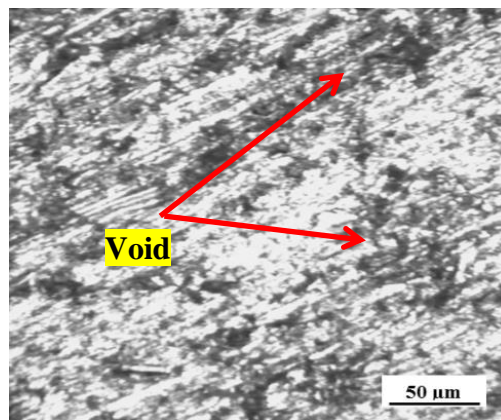
Metallographic image for 1200 RPM, traverse speed 45mm/min and straight cylindrical pin combination



Metallographic image for 1400 RPM, traverse speed 15mm/min and square pin combination



Metallographic image for 1400 RPM, traverse speed 30mm/min and straight cylindrical pin combination



Metallographic image for 1400 RPM, traverse speed 45mm/min and taper cylindrical pin combination

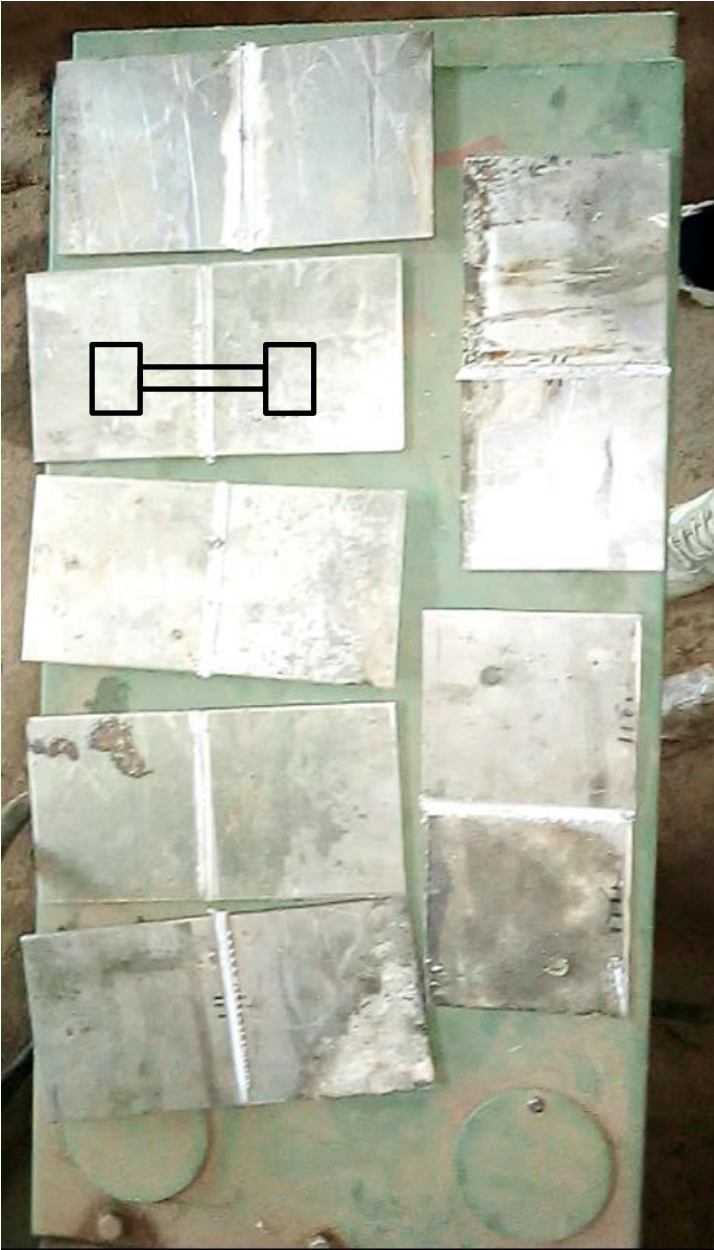
Appendix 4: Liquid penetrant test results



Appendix 5: Experimental operation in Workshop



Appendix 6: weld samples



Appendix 7: Tensile test operation using UTM

